Technical Report Documentation Page

1. Report No. ABC-UTC-2016-C4-UW01-Final	2. Government Accession No.	3. Recipient's Catalog No.	
4. Title and Subtitle **Exploring Fiber-Reinforced Polymer Concrete for Accelerated Bridge Construction Applications**		5. Report Date May 2024 6. Performing Organization Code	
7. Author(s) Carolyn Donohoe, Travis Thonstad (https://orcid.org/0000-0002-1575-3617)		8. Performing Organization Report No.	
9. Performing Organization Name and Address Department of Civil and Environmental Engineering University of Washington, Box 352700 Seattle, WA 98195-2700		10. Work Unit No. (TRAIS) 11. Contract or Grant No. 69A3551747121	
12. Sponsoring Organization Name and Address Accelerated Bridge Construction University Transportation Center Florida International University 10555 W. Flagler Street, EC 3680 Miami, FL 33174	US Department of Transportation Office of the Assistant Secretary for Research and Technology And Federal Highway Administration 1200 New Jersey Avenue, SE Washington, DC 201590	13. Type of Report and Period Covered Final Report (March 2017- May 2024) 14. Sponsoring Agency Code	
15. Supplementary Notes Visit www.abc-utc.fiu.edu for other ABC reports.			
16. Abstract This experimental program investigated the non-contact splice strength of epoxy-coated deformed bar reinforcement embedded in a commercially available fiber-reinforced polymer concrete (FRPC) to assess its suitability as a closure pour material. The test series examined the effects of embedment length, side cover, bar size, and test temperature on the non-contact splice strength. A statistical analysis of the collected data supports the use of similar joint geometries as currently recommended for ultra-high-performance concrete (UHPC) for in-service temperatures less than or equal to 110 °F. The capability to use the same joint geometry for FRPC as UHPC helps increase the potential options for a given ABC project.			
17. Key Words polymer concrete; closure joint; accelerated bridge construction; prefabricated bridge elements; precast concrete; non-contact splice; bond strength		18. Distribution Statement No restrictions.	
19. Security Classification (of this report) Unclassified.	20. Security Classification (of this page) Unclassified.	21. No. of Pages 71	22. Price

Form DOT F 1700.7 (8-72) Reproduction of completed page authorized

(this page is intentionally left blank)

Exploring Fiber-Reinforced Polymer Concrete for Accelerated Bridge Construction Applications

Final Report

May 2024

Principal Investigator: Travis Thonstad

Department of Civil and Environmental Engineering
Florida International University

Authors
Carolyn Donohoe, Travis Thonstad

Sponsored by
Accelerated Bridge Construction University Transportation Center

A report from
Department of Civil and Environmental Engineering
Florida International University
10555 West Flagler Street, EC 3680
Miami, FL 33174
Phone: 305-348-2824 / Fax: 305-348-2802
https://cee.fiu.edu/

DISCLAIMER

The contents of this report reflect the views of the authors, who are responsible for the facts and the accuracy of the information presented herein. This document is disseminated in the interest of information exchange. The report is funded, partially or entirely, by a grant from the U.S. Department of Transportation's University Transportation Program. However, the U.S. Government assumes no liability for the contents or use thereof.

CONTENTS

LIST OF FIGURES

LIST OF TABLES

ACKNOWLEDGMENTS

This project was supported by the Accelerated Bridge Construction University Transportation Center (ABC-UTC at www.abc-utc.fiu.edu) at Florida International University (FIU), as lead institution, and Iowa State University (ISU) and the University of Nevada-Reno (UNR) as partner institutions. The authors would like to acknowledge the ABC-UTC support. The authors would like to extend special appreciation to the ABC-UTC and the U.S. Department of Transportation Office of the Assistant Secretary for Research and Technology for funding this project.

The authors would like to thank Research Advisory Panel members Anthony Mizumori (WSDOT), Duane Carpenter (NYDOT), and Steve Seguirant (Concrete Technology Incorporated) for their contributions to the research program; Kwik Bond Polymers for their in-kind contribution of the HCSC material used in the test specimens; and Casey Rafter and Dan Uldall from Kwik Bond Polymers for their technical assistance throughout the project.

CHAPTER 1: INTRODUCTION

1.1. Project Motivation

The use of precast concrete superstructure elements is a popular strategy for accelerated bridge construction (ABC) and rehabilitation projects. The major advantage is that precast concrete elements can be fabricated before, or in parallel with, on-site activities, thus expediting project delivery. To complete the superstructure, closure joints between adjacent precast superstructure elements are filled with a field-cast material, creating continuity between the concrete elements and splicing steel reinforcement that protrudes from the precast members into the joints. These joints can be longitudinal, parallel to the direction of traffic, when a bridge span comprises multiple adjacent decked girders or transverse, perpendicular to the direction of traffic, when full-width deck panels are used to form the bridge superstructure. These configurations are shown schematically in Figure 1-1. The geometry of the closure joints, the speed at which the connections can be completed, how long before the bridge can be opened to traffic, and the cost of the system are all dependent on the material that is used to fill the gaps between precast elements. The closure joint material must possess strength and durability equal to or better than the adjacent concrete and must be capable of transferring the tensile forces between reinforcement from adjacent elements.

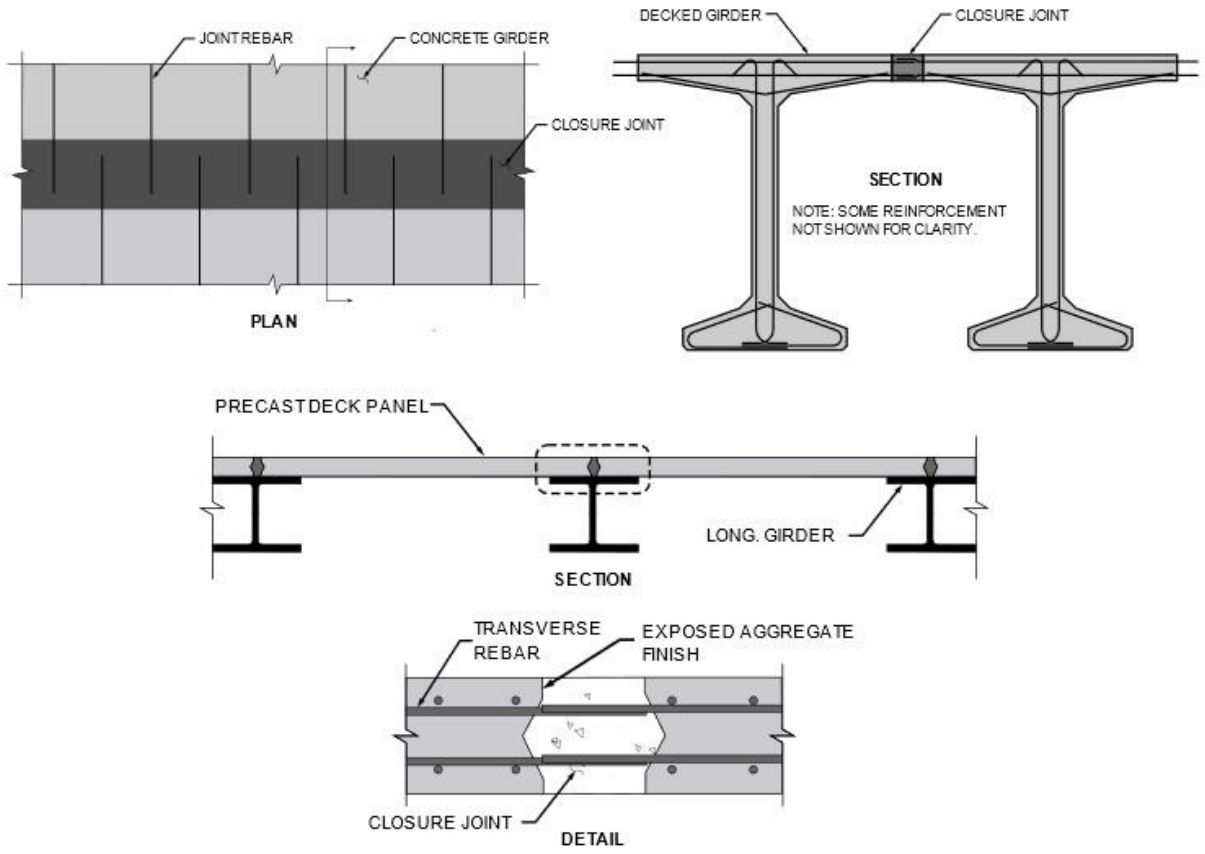

Figure 1-1. Precast concrete girder closure joint plan and section (adapted from Peruchini et al. 2017) and precast deck panel closure joint section and detail

Presently, the most common material used in closure joints is ultra-high performance concrete (UHPC). The tension and bond strengths of UHPC make it an excellent choice as a closure joint material. As bridge designers and owners have become more comfortable with the unique design and construction of UHPC and ABC, its use in bridge projects has increased exponentially, as shown in Figure 1-2 for the decade between 2006 and 2016

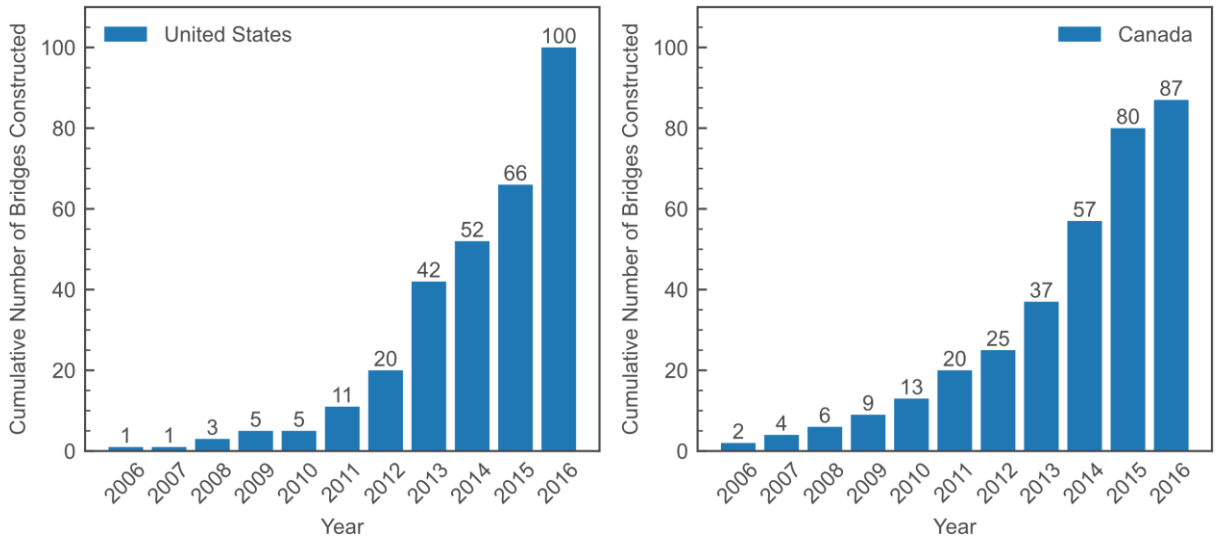

Figure 1-2. Timeline of UHPC usage in bridge construction in (a) the United States, (b) Canada. Data from Haber et al. (2018)

The properties and capabilities of specific UHPC mixes have been extensively studied, most prominently at the Federal Highway Administration (FHWA) and Accelerated Bridge Construction University Transportation Center (e.g., Graybeal 2006, Graybeal 2014, Haber et al. 2018, Peruchini et al. 2017, Shahrokhinasab and Garber 2021), and are relatively well understood. However, most ABC and other construction projects rely on proprietary UHPC materials, at the contractor's request. This provides a lower risk to the contractor as the material supplier often comes to the site and takes responsibility for the batching and mixing but increases the cost of the closure pour. While UHPC may still provide the best solution in many instances, alternative materials exist with similar mechanical properties that may prove advantageous in certain applications.

For example, the time at which UHPC achieves its design strength is directly proportional to the rate of hydration of the cementitious binder. If rapid strength gain is needed, perhaps to complete the work in a short closure window, alternative joint materials that utilize polymer binders, instead of cementitious ones, may be more suitable. Polymer concretes (PCs) have the advantage of requiring shorter closure windows (approximately 4 hours versus 72 hours of UHPC) due to the very rapid strength gain of the polymer, which could be ideal for overnight construction or rehabilitation projects. Similar to traditional cementitious concretes, PCs are composed of a mix of aggregates and binder, however PCs do not contain hydrated cement paste, instead hardening and gaining strength through the cross-linking of polymer chains. Polymer concretes can be tailored to have a variety of properties depending on the formulation of the polymer used, including rapid curing at ambient temperatures, high tensile and flexural strength, good chemical resistance,

and good adhesion to most surfaces (ACI 2019). Fiber-reinforced polymer concrete (FRPC), which contain microfibers to modify the mechanical properties of material, display levels of two critical characteristics (bond and tension strength) that are comparable to, or potentially better than, those of UHPC. The use of FRPC may provide an additional option to the engineer and contractor when choosing a closure joint material for a particular circumstance.

Polymer concrete has been used as a non-structural and overlay material in the United States since the 1950s (ACI 2019, Fowler 1999, Maas 1997). Many advancements in material composition, packaging, and construction practices have led to substantial improvements in PC quality and performance (Maas 2003, Fowler and Whitney 2012). Figure 1-3 shows the use of polyester polymer concrete (PPC) as an inlay and overlay material in Spokane, Washington (Anderson et al. 2013). Multiple state's department of transportation utilize PC overlays, most notably California and New York. PC overlays are durable and provide high protection against moisture and chloride ions from deicing salts (Maas 2003). They are also resistant to cracking and delamination and have service life of up to 20 years, longer than other traditional overlays (Sprinkel 2003).

Figure 1-3. (a) Wheel path PPC inlay, (b) PPC overlay with diamond grinding (Anderson et al. 2013)

Despite being used as an overlay material for over 40 years, there are few examples of PC used for closure joints or other full-depth repairs. Previous studies investigating PCs for closure joints between precast deck panels found that specimens constructed with PC closure joints had similar strengths and lower initial stiffnesses than those constructed with UHPC (Moustafa et al. 2019). Mantawy et al. (2019), studied the bond and splice characteristics of a polymethyl methacrylate polymer concrete and found that the bond strength was higher, and the splice length was shorter, for the specimens containing PC in comparison with those containing UHPC.

The addition of fibers to PCs leads to improved properties that could lead to smaller and simpler joint geometries when compared with UHPC or polymer concretes without fibers. There is the potential for smaller closure windows than when using UHPCs due to the faster strength gain of the polymer. This hesitancy in the use of FRPC closure joints by bridge owners and agencies is largely due to the sparsity of experimental data and the lack of specific design guidance that accounts for the unique mechanical properties of FRPC in these applications. Further experimental

investigation into the FRPC's mechanical and bond properties is crucial to understanding its capabilities in structural and ABC usage.

1.2. Research, Objectives, and Tasks

The primary objectives of this research project were the following:

1. review the most promising FRPC materials,
2. assess the temperature dependent properties of FRPC behavior,
3. characterize the mechanical properties (tensile, flexural, compressive) of FRPC, and
4. characterize the splice performance of deformed bars embedded in FRPC materials.

These objectives were accomplished through the following research tasks:

- *Task 1 – Literature Review*: Previous research on fiber reinforced polymer concrete has been compiled and separated into areas of interest pertinent to bridge construction applications.
- *Task 2 – FRPC Material Characterization*: The mechanical properties of a commercially available FRPC material, Kwik Bond Hybrid Composite Synthetic Concrete (HCSC), were determined at several test temperatures and ages using standard test methods that would be part of a typical quality control program (i.e. compressive strength, tension strength, and anchorage strength).
- *Task 3 – Testing of Splice Specimens:* The tests investigated a simplified, non-contact splice configuration that isolates the behavior of reinforcement in a closure joint. The specimen size was selected to allow conditioning the specimens to different temperatures using conventional laboratory equipment and tested using a universal testing machine under precise displacement control. The variables that were investigated include the temperature at time of testing, overlap length between bars, side cover, and bar size
- *Task 4 – Development of Design Recommendations*: The *AASHTO LRFD Guide Specifications for Accelerated Bridge Construction* (AASHTO 2018) recommends a minimum embedment length for deformed bar reinforcement in UHPC, ℓ_d, of $8d_b$ for #8 bars or smaller with f_y less than or equal to 75 ksi and clear cover greater than or equal to $3d_b$. The splice length for straight deformed steel reinforcement is recommended to be at least 0.75 ℓ_d. The results of the non-contact splice tests support using HCSC in closure joints with identical geometries as those recommended for UHPC for service temperatures in the range of 0-110 °F. The capability of HCSC to permit the same joint geometry as UHPC would help increase the potential closure pour options for a given ABC project, especially when rapid strength gain is beneficial.

1.3. Research Advisory Panel (RAP)

The project work was done in collaboration with the Research Advisory Panel (RAP). The following people participated in the RAP:

- Anthony Mizumori (WSDOT)
- Duane Carpenter (NYDOT)
- Steve Seguirant (Concrete Technology Incorporated)

1.4. Report Overview

The report is organized as follows:

- **Chapter 2.** Literature Review: summarizes past experiments conducted on polymer concrete with varying mix designs and their associated mechanical properties
- **Chapter 3.** Material Characterization: presents the mixture design, mixing and casting procedure, and testing plan for compression, flexural beam, and bond pullout testing. Tests included strength gain over time and different testing temperatures.
- **Chapter 4.** Non-Contact Splice Testing Program: explains the experimental design, specimen geometry, and specimen parameters used for the non-contact splice specimen testing, including the construction sequence, specimen monitoring, and test procedure for the testing of the influence of primer, geometric, and temperature parameters.
- **Chapter 5.** Results: presents the results of the non-contact splice testing program are through tables, plots, and photos. Presents a statistical analysis of the collected data focusing on the influence of temperature, splice length, side cover, and bar size
- **Chapter 6.** Design Recommendations: provides preliminary recommendations for longitudinal joint geometry with guidance for required splice length and side cover.
- **Chapter 7.** Summary, Conclusions, and Future Work: summarizes the completed work, draws conclusions based on the results of the study, and presents recommendations for future work.

CHAPTER 2. LITERATURE REVIEW

The behavior of polymer concrete is highly dependent on the chemistry of the binder. Other important factors include the proportioning of binder and aggregates in the mixture and the aggregate composition and type. Several binders are commonly used and commercially available for polymer concrete including epoxy, methacrylate, and polyester. Figure 2-1 summarizes the chemical process that occurs for a generic polyester-based polymer concrete, as an example. This particular pathway is popular in commercial applications because the two-part mixing process is simple for the installer, yet still allows adjustments for project and site-specific needs.

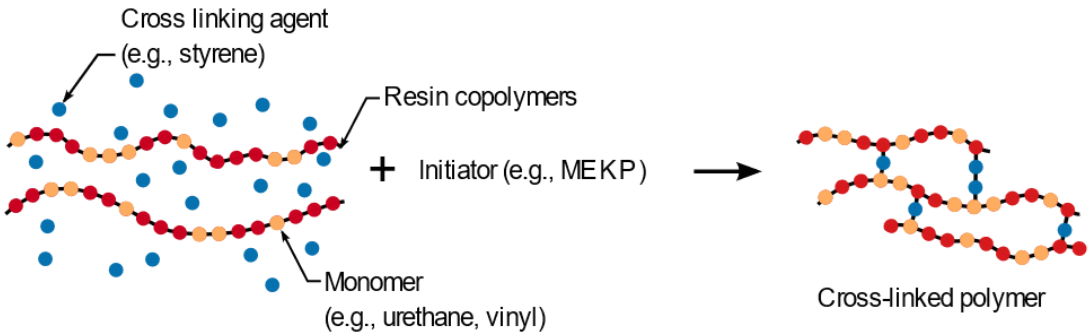

Figure 2-1. Schematic of polymerization and cross-linking

Prepackaged mixtures commonly have the resin polymers in solution with the monomer cross-linking agent. When mixed with an initiator, the monomer and polymer chain form a cross-linked polymer with the monomer providing the link between the polymer chains. The cross-linking process is exothermic, increasing material temperature as it gels and hardens. This process creates a thermoset polymer, a polymer that will solidify when cured that cannot be remolded due to the irreversible cross-linked bonds. The cross-linked polymer physically binds the aggregate, creating a cohesive material.

Cost, durability, adhesion to aggregate, and ease of polymerization at room temperature all play a role in the selection of the monomer type. Inhibitors and accelerators can be included to tune the time when the mixture reaches a gel point and workability is severely reduced, in response to on-site conditions such as ambient temperature, complexity of the pour, etc. Additives such as plasticizers, colorants, and flame retardants can also be included to modify the workability, mechanical properties, or appearance.

2.1. Mechanical Properties

The material properties of PCs are highly dependent on mix design, curing method, age, testing conditions, and procedures (Vipulanandan and Paul 1990). However, the variation in properties of test specimens from different batches within one mix design is typically small (ACI 2019). Table 2-1 summarizes material properties from various studies.

Figure 2-2 compares the compressive stress-strain behavior of several polymer concretes available in the literature. The stress-strain behavior for conventional concrete and ultra-high-performance concrete are also included for reference. Compressive behavior is shown here because it is the most widely reported and is used as a design basis for structural concrete members; however, similar plots could be constructed for flexural or tensile strengths with similar observations made. In general, polymer concretes can be designed with comparable or higher compressive strengths

than conventional cementitious concrete at room temperature. Ranges in compressive strength are dependent on the binder, aggregate size, type, and gradation.

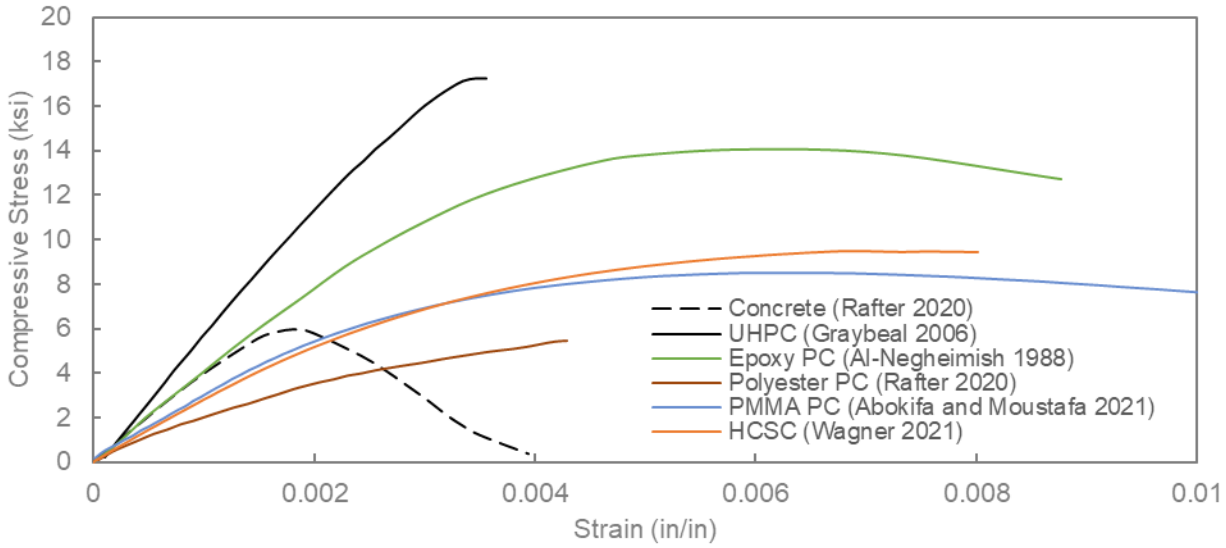

Figure 2-2. Compressive stress-strain behavior of polymer concretes at room temperature

PCs typically have higher flexural and tensile strengths than cementitious concrete, with lower flexural moduli. The flexural strength of PC is highly dependent on the choice of polymer. Generally, highly cross-linked polymers result in higher flexural strengths. Hsu (1984), found that the modulus of rupture for PC varied linearly with the square root of compressive strength, similar to that of cementitious concrete.

Deformation of materials under load is dependent on the modulus of elasticity of the composite material. For PCs, the modulus of elasticity is highly dependent on the modulus of the polymer binder (ACI 2019). The high compressive strengths of PCs are achieved at much larger strains than cementitious concretes, and therefore polymer concretes tend to exhibit lower elastic moduli when compared with conventional cementitious concrete. Additionally, the mechanical properties of polymer concretes vary considerably with temperature, strain rate, and load duration.

Table 2-1. Mechanical properties from previous polymer concrete studies

Author	Resin	Compressive Strength (psi)	Modulus of Elasticity (ksi)	Modulus of Rupture (psi)	Bond Strength (psi)	Tensile Strength (psi)
Abdel-Fattah and El-Hawary 1999	Epoxy	% Resin by weight 9% = 5200, 12% = 5500, 15% = 3200	-	% Resin by weight 9% = 1300, 12% = 1500, 15% = 700	-	-
Abdel-Fattah and El-Hawary 1999	Epoxy	% Resin by weight 9% = 9100, 12% = 10400, 15% = 9300,	-	% Resin by weight 9% = 1900, 12% = 2200, 15% = 1800,	-	-
Abdel-Fattah and El-Hawary 1999	Polyester	% Resin by weight: 9% = 8000, 12% = 10400, 15% = 9100	-	% Resin by weight 9% = 1500, 12% = 2000, 15% = 1700	-	-
Abokifa and Moustafa 2021	PMMA (Transpo T-17)	9000	2800	-	-	-
Al-Negheimish 1988	Epoxy	13600	3650	3100	-	-
Guedes et al. 2004	Epoxy	11900	1668	5600		-
Hassani Niaki et al. 2018	Epoxy	13600	-	5700	-	1700
Hong 2017	Epoxy	6000	-	3400	600	-
Hsu 1984	PMMA	9800	3240	2000	-	1300
Kwik Bond Polymers 2020a	Proprietary (HCSC)	10000	2500	2500	-	1500
Kwik Bond Polymers 2020b	Polyester (PPC 1121)	6000	1500	2000	700	800
Mani et al. 1987	Epoxy, polyester	Epoxy: 10400 Polyester: 6000	-	Epoxy: 3000 Polyester: 1800	-	-
Mantawy et al. 2019	PMMA	10500	-	-	-	1000
Mebarkia and Vipulanandan 1992	Polyester	10% PC, 6% fibers: 4800, 18% PC, 4% fibers: 12200	-	-	-	-

Author	Resin	Compressive Strength (psi)	Modulus of Elasticity (ksi)	Modulus of Rupture (psi)	Bond Strength (psi)	Tensile Strength (psi)
Oussama et al. 2012	Epoxy	% Resin by weight 6% = 3600, 9% = 5300, 13% = 12400, 16% = 13300		1800 2900 3400 3500	-	-
Reis 2005	Epoxy (Silicem Eposil 551), Masterflow 211, Emaco S88, Groutek S, Hagenpox	8700, 7400, 6500, 6500, 7200	1600	-	-	-
Ribeiro et al. 2004	Epoxy, polyester	-	-	Epoxy: 6100, Polyester: 3500	-	-
Sett and Vipulanandan 2004	Polyester	% Resin by weight 14% = 8000, 18% = 7600, 20% = 8600	-	-	-	14% = 1000
Toufigh et al. 2016	Epoxy (NITOBOND-EP, ML506-HA32, PR700-PH500)	9400 5200 5100	-	-	-	-
Vipulanandan and Mebarkia 1996	Polyester	-	-	2400	-	-
Vipulanandan and Paul 1990	Epoxy, polyester	Epoxy: 7400 Polyester: 7000	-	-		-
Wagner 2021	Proprietary (HCSC)	9000	2700	-	-	-

2.2. Effect of Temperature

The influence of temperature on the properties of polymer concretes is of particular interest for ABC applications. The temperature at curing also affects the mechanical properties of PC, as the chemical reaction of cross-linking is dependent on temperature. At high temperatures, the reaction occurs too rapidly, and the elements of the reaction do not have adequate time to mix before the reaction occurs. At low temperatures, the reaction occurs too gradually, which prevents proper curing (Oussama et al. 2012).

In general, the strength of polymer concretes varies inversely with temperature. At lower temperatures, polymer concretes have higher strengths and elastic moduli and lower strain capacities when compared to the properties at room temperature. The reverse is true at higher temperatures. While this trend holds for all polymer concretes, the variation in mechanical properties as a function of temperature depends significantly on the binder chemistry. Understanding the variation in mechanical properties with temperature for commercially available polymer concretes is critical for determining design recommendations for ABC closure joint applications. Figure 2-3 shows the influence of testing temperature on the compressive strength of several polymer concretes.

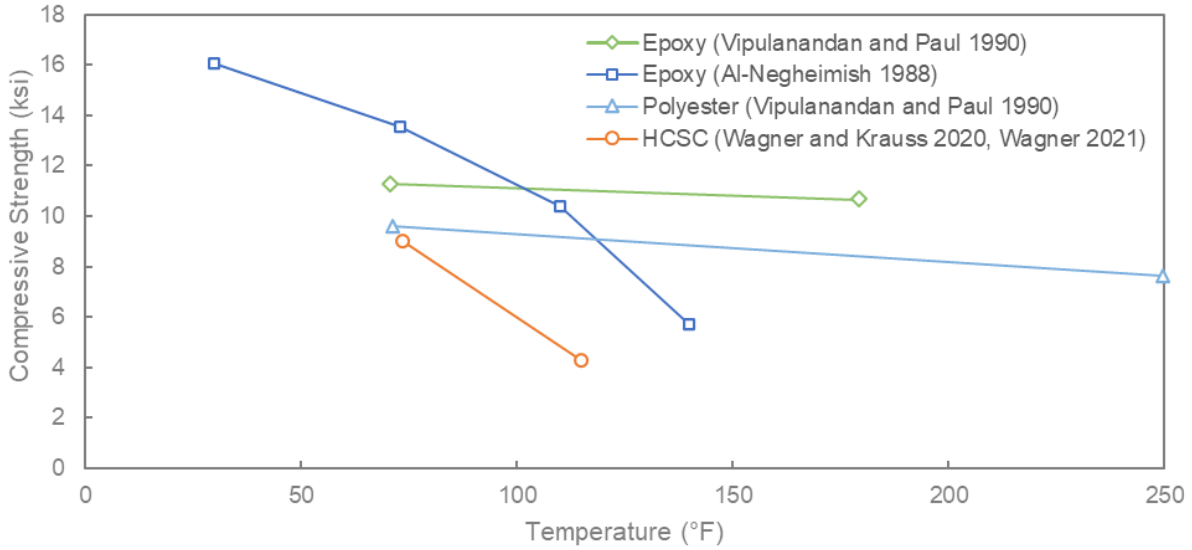

Figure 2-3. Influence of temperature on compressive strength of polymer concretes

Table 2-2 summarizes previous experimental campaigns that have considered the influence of temperature on the mechanical properties of polymer concretes. Researchers have investigated the influence of temperature at several different stages: during curing or hardening of the polymer binder, freeze/thaw cycling, exposure to extreme temperatures prior to testing at ambient conditions, and during the testing itself.

In addition to affecting the mechanical properties, changes in temperature can also cause stresses to develop at PC-reinforced concrete interface, since the coefficient of thermal expansion for PCs is typically higher than that of cementitious concretes. PCs with low resin content, around less than 10% by weight, are more influenced by aggregate and have lower expansion coefficients (ACI 2019). As polymer content increases, the coefficient of thermal expansion approaches that of the polymer.

Table 2-2. Previous studies investigating the effect of temperature

Author	Resin/ Fibers	Temp Type	Key Findings
Aboutaha et al. 2005	Transpo T48A (epoxy), Flexolith (epoxy), Redeck, Strongwell, with fibers	Testing temperature	• Compressive strength and modulus of PC are higher at low temperatures and lower at high temperatures compared to room temperature. • The flexural modulus of PC increases at low temperatures and decreases at high temperatures.
Al-Negheimish 1988	Epoxy	Testing temperature	• The compressive strength of PC decreases with increases in temperature. The trend is linear between 30 °F and 110 °F with sharper decreases after 140 °F • The modulus of elasticity decreases with increases in temperature • At higher temperatures, the stress-strain curve becomes nonlinear at lower percentages of ultimate strength
Heidari-Rarani et al. 2014	Epoxy, with E-glass fibers	Freeze-thaw cycles, thermal fatigue cycles	• Freeze/thaw cycles did not change the failure mode type • Heat to cool thermal cycles increased the durability and load-bearing capacity whereas the cool to heat thermal cycles increased the risk of brittle tensile fracture • Fracture toughness was more sensitive to higher mean temperature cycles, where tensile strength was more influenced by lower mean temperature cycles
Hong 2017	Epoxy	Curing temperature	• Rapid strength gain occurs in the first 24 hours of curing, with 27% of the compressive strength after 6 hours and 70% after 24 hours for room temperatures • Higher curing temperatures increase the initial strength due to the increased rate of the reaction but has a negative effect on the final strength • Flexural strength decreased with an increase in curing temperature. Slow decreases in the strength up to 20 °C then a rapid decrease • The reinforcement bond strength exceeded the ACI recommendation of 1.7 MPa up to a curing temperature of 60 °C • Flexural strengths were highest at -10 °C and decreased with an increase in curing temperature. Specimens above 40 °C were insufficient per ACI recommendations • There is a strong correlation coefficient between compressive strength and

Author	Resin/ Fibers	Temp Type	Key Findings
			bond and flexural strength, indicating that the bond and flexural strength can be used to draw a general conclusion from only compression strength data.
Krauss and Lawler 2018	Polyester Polymer Concrete (PPC)	Testing temperature	• For a #6 bar, bar yield or breakage occurred for embedment of 4.5 and 7.5 in ($6d_b$ or greater) at room temperature. For elevated temperatures (110 °F) the reinforcement pulled out before yielding was achieved. At an embedment of $7.5d_b$ and 3in side cover, the reinforcement had an average stress of 67700 psi at the time of pullout failure. • As embedment length increased, the bar stress at failure increased. • No significant difference in failure stress of the PC was noted for specimens with epoxy coated versus uncoated reinforcement
Oussama et al. 2012	Epoxy	Exposure temperature	• After being exposed to temperatures greater than 150 °C, the epoxy polymer displays a loss of strength, primarily due to thermo-oxidative degradation and debonding between the binder and aggregate. • After high-temperature exposure, there are significant reductions in compressive strength, up to 50% loss after exposure to 250 °C. • Increases in flexural strength were reported until 150 °C, then a reduction in strength was found. The behavior of the samples became more brittle with high-temperature exposure
Reis and Ferreira 2006	Epoxy, with glass and carbon fibers	Freeze-thaw cycles, thermal fatigue cycles	• With increases in peak temperature, the flexural elasticity decreases, and failure is more ductile, resulting in higher fracture toughness. • The high peak temperature also results in a loss of mechanical strength, due to the degradation of the cohesion between polymeric chains.
Ribeiro et al. 2003a	Epoxy, polyester, with glass and carbon fibers	Thermal expansion thermal cycle	• At higher temperatures, the coefficient of thermal expansion is higher. And at temperatures above 10 °C, the increase rate for epoxy PC is higher than polyester PC • The addition of glass fibers had no significant influence on the coefficient of thermal expansion, while carbon fibers had a strong reducing effect. • The coefficient of thermal expansion varies via a polynomial law and

Author	Resin/ Fibers	Temp Type	Key Findings
			therefore varies continuously between -15 °C and 60 °C
Ribeiro et al. 2003b	Epoxy, polyester	Curing temperature and duration	• The curing cycle does not influence the final mechanical properties, but the time required varies with temperatures. Seven days curing at room temperature was shown to be equivalent to three hours at 80 °C.
Ribeiro et al. 2004	Epoxy, polyester	Testing temperature, conditioning temperature	• Freeze/thaw cycles between -10 °C and 10 °C resulted in little damage, potentially due to the reduced degree of water adsorption and water content • Flexural properties are highly dependent on temperature, with epoxy being more sensitive than polyester • Temporary changes in temperature have no significant influence on the flexural strength as long the specimen is returned to the original temperature.
Vipulanandan and Paul 1990	Epoxy, polyester	Curing temperature, testing temperature	• Splitting tensile strength of epoxy PC is almost unchanged but increases with curing temperature for polyester PC. • The compressive strength ratio (strength of the PC/strength of just polymer) increases with increases in temperature.
Wagner and Krauss 2020	Hybrid Composite Synthetic Concrete (HCSC)	Testing temperature	• NYSDOT pull-out tests at elevated temperatures were sufficient to develop yield stress for the tested bars and embedment length • The compressive strength of HCSC at elevated temperatures is less than the strength at room temperature.

2.3. Reinforcement

As an additional tool for the modification of polymer concrete behavior, fibers can be added to the mixture of binder and aggregate. Fibers have been shown to increase the splitting tensile strength and ductility of polymer concretes and decrease the coefficient of thermal expansion, which is typically higher than that of conventional concrete and steel (ACI 2019). Possible fiber materials include steel, glass, basalt, and other recycled materials. Numerous studies using epoxy and polyester PC with glass, carbon, or steel fibers have been conducted and are summarized in Table 2-3.

Although polymer concretes have tensile strengths exceeding those of conventional cementitious concrete (by roughly a factor of two), deformed bar reinforcement is necessary for typical structural applications. In closure joints, adequate bond between the closure pour material and deformed bar reinforcement is, therefore, crucial. The required development and splice length of the bars must be long enough to develop the yield stresses in the reinforcement. While much is known about the required development lengths in conventional concrete, very little research has been conducted on the structural use of PCs. Mantawy et al. (2019) conducted pull out tests and spliced beams tests for deformed bars embedded in Polymethyl methacrylate (PMMA) at room temperature. They found that the minimum development length for deformed bars was between 3.6db and 4.1db and the minimum required splice length was 4.1db, with a concrete cover of 3db. These development and splice lengths are significantly smaller than the AASHTO requirement for conventional concrete and on the same order as that of UHPC. Abokifa and Moustafa (2021) tested PMMA and UHPC closure joint deck specimens under flexural loading. Both deck specimens utilized splice lengths of 8db. They found that PMMA adequately satisfies the AASHTO LRFD requirements for longitudinal joints at room temperature. Both deck systems remained elastic without any major flexural or interface cracking in the joint. When UHPC joint geometry recommendations were used with PMMA, the results also met AASHTO LRFD standards. This indicates the field joint width for UHPC is also sufficient for PMMA in terms of load distribution.

Table 2-3. Previous studies investigating the influence of fibers

Author	Resin	Reinforcement/Fibers	Findings
Aboutaha et al. 2005	Transpo T48A (epoxy), Flexolith (epoxy), Redeck, Strongwell	Varies with proprietary blend	• Compressive strength and modulus of PC are higher at low temperatures and lower at high temperatures compared to room temperature • The flexural modulus of PC increases at low temperatures and decreases at high temperatures.
Heidari-Rarani et al. 2014	Epoxy	E-glass fibers (0.5% by weight)	• Freeze/thaw cycles did not change the failure mode type • Heat to cool thermal cycles increased the durability and load-bearing capacity whereas the cool to heat thermal cycles increased the risk of brittle tensile fracture • Fracture toughness was more sensitive to higher mean temperature cycles, where tensile strength was more influenced by lower mean temperature cycles
Reis and Ferreira 2006	Epoxy	Glass fibers (1% by weight), carbon fibers (2% by weight)	• With increases in peak temperature, the flexural elasticity decreases, and failure is more ductile, resulting in higher fracture toughness. • The high peak temperature also results in a loss of mechanical strength, due to the degradation of the cohesion between polymeric chains.
Ribeiro et al. 2003	Epoxy, polyester	Glass fibers (1% by weight), carbon fibers (2% by weight)	• At higher temperatures, the coefficient of thermal expansion is higher. And at temperatures above 10 °C, the increase rate for epoxy PC is higher than polyester PC • The addition of glass fibers had no significant influence on the coefficient of thermal expansion, while carbon fibers had a strong reducing effect. • The coefficient of thermal expansion varies via a polynomial law and therefore varies continuously between -15 °C and 60 °C
Abdel-Fattah and El-Hawary 1999	Epoxy, polyester	Uncoated rebar	• Maximum compressive strength and modulus of rupture were achieved with 12% resin content for all types of resin tested

Author	Resin	Reinforcement/Fibers	Findings
			• The modulus of rupture can be up to 3 times that of Portland-cement concrete of the same ultimate compressive strength
Abokifa and Moustafa 2021	Transpo T-17 (Methyl Methacrylate)	Uncoated rebar	• PMMA reached the AASHTO ultimate load before significant cracking was observed • PMMA has a larger compressive ultimate strain, enhanced post-peak behavior, and strain deformation capacity than portland-cement concrete and UHPC • PMMA is ductile and has a sustained tensile capacity with increasing strain until cracking. Failure of PMMA in tension is brittle after the first crack is formed.
Guedes et al. 2004	Epoxy	GFRP Bar	• PC displays a linear viscoelastic mechanical behavior with the GFRP-reinforcement exhibiting linear elastic mechanical behavior for a stress level up to 45% of the ultimate load • The created model predicted a strong increase of GFRP-rebar tensile strength after 10000 hours, with the suggested consideration of creep and creep rupture of the rebar for long-term analysis
Mantawy et al. 2019	Polymethyl Methacrylate	Gr 60 uncoated rebar	• Recommended development length of 3.6-4.1 db in PMMA • Minimum lap splice length of 4.1db recommended with a cover of 3db
Mebarkia and Vipulanandan 1992	Polyester	Glass fibers, 0-6% by weight	• An increase of fibers results in a reduction of the compressive modulus and an increase in compressive strength of 33% over unreinforced PC • Glass fibers increase the failure strain and toughness
Park et al. 2010	Polyester	Gr 60 uncoated rebar	• The actual moment of inertia of PC beams is underestimated via the ACI effective moment of inertia • The ductility indexes decrease as the ratio of tensile

Author	Resin	Reinforcement/Fibers	Findings
			reinforcement increases
Reis 2005	Silicem eposil 551 (Epoxy)	Glass fibers (1% by weight), carbon fibers (2% by weight)	• The addition of fibers increases the compressive strength compared to unreinforced PC. Glass fibers resulted in an increase of 27.5-45.4% and 36.1-55.1% for carbon fibers. • Fibers also result in a slightly more ductile failure; unreinforced PC displays a brittle failure
Sett and Vipulanandan 2004	Polyester	Glass fibers, carbon fibers, 0-6% by weight	• The optimum polymer content is 14% when unreinforced. With 6% glass fibers, 18% polymer is optimal for strength and workability. For 6% carbon fibers, 20% polymer is optimal for workability and tensile strength. • Tensile strength of PC is improved by 85% and 60% from the addition of 6% fibers, glass, and carbon respectively. • Glass fibers improved the compressive strength of PC, but carbon fibers did not have a significant difference • Both types of fibers increased the damping ratio for longitudinal modes
Vipulanandan and Mebarkia 1996	Polyester	Glass fibers, 0-6% by weight	• The addition of 6% glass fibers with 18% polymer content resulted in an 80% increase in flexural strength compared to unreinforced PC. • Silane-treated aggregates and fibers doubled the flexural strength for a mix including 6% glass fibers and 18% polymer content. • Based on the stress intensity factor, crack resistance curved can be linearly approximated

CHAPTER 3. MATERIAL CHARACTERIZATION

The research program was broken down into two phases – the first of which was to characterize the mechanical properties of a commercially available FRPC material (compression strength, compression modulus, flexural strength, and tension strength) at several test temperatures and ages using standard test methods that would be part of a typical quality control program.

The use of commercially available products was preferred so that the results of the research were scalable. A commercially available FRPC material was identified, Kwik Bond Polymers' Hybrid Composite Synthetic Concrete (HCSC). HCSC comprises a urethane vinyl ester hybrid copolymer resin binder, graded silica aggregates, and pre-blended basalt chopped fibers. The initiator used is MEKP and the accelerator is a propriety blend, "Z-cure". An HMWM primer was used in conjunction with the binder for bonding HCSC to concrete and steel substrates. Table 3-1 compares the manufacturer provided mechanical properties of HCSC to UHPC and other commercially available polymer concretes.

Table 3-1. Summary of PPC and HCSC mechanical properties

Material (Manufacturer)	UHPC	MMA (Transpo)	PPC (Kwik Bond)	HCSC (Kwik Bond)
Compressive Strength	24000 psi	9000 psi	6000 psi	10000 psi
Tensile Strength	1200 psi	1200 psi	800 psi	1500 psi
Modulus of Elasticity	7000 ksi	1200 ksi	1500 ksi	2500 ksi
Coefficient of Thermal Expansion	6-8 x 10^{-6} in/in/°F	-	<10 x 10^{-6} in/in/°F	<11 x 10^{-6} in/in/°F
Development Length	~8 d_b	~4+* d_b	~6* - 10** d_b	~6** d_b

*At room temperature, ** At elevated temperature

3.1. Polymer Concrete

Table 3-2 summarizes the mixture design recommended by the manufacturer that were used in this study. Each test series was cast with one mixed batch of approximately 230 lb of prebagged aggregate and basalt fiber mix.

Table 3-2. HCSC mixture design

% Binder (by mass Aggregate)	% MEKP (by mass Binder)	% Z-cure (by volume MEKP)
13.5%	2.20%	3.00%

For the bond tests that included deformed bar reinforcement, a HMWM primer was applied to the bar surface before casting HCSC per the manufacturer's recommendation. The HMWM primer was mixed with cumene hydro peroxide (CHP) as the initiator and the proprietary Z-cure accelerator in a 128-3-1 volume ratio. The primer was applied in a thin coat using a foam brush and allowed to cure for at least 30 minutes before casting the HCSC.

Table 3-3 shows the working time and time to 70% of the 7-day compressive strength when cylinders were cured at room temperature, for three levels of accelerator, measured as a volume ratio to the initiator. The volume of the accelerator can be adjusted to achieve a range of working and curing times or to accommodate specific site conditions (i.e. cold or hot weather). At the start of the project, several trial batches were performed to determine the appropriate level of the

accelerator to use for the remainder of the test series. The table clearly shows the tradeoff between working time and the time required to achieve strength. If shorter working times can be tolerated, significant strength (70% of the 7-day value) can be achieved 2 hours after mixing. In the laboratory, a value of 3% accelerator by volume initiator was selected as a compromise between working time and time required for predetermine strength gain.

Table 3-3. Normalized compressive strength and working time for various accelerator volumes

Accelerator by volume initiator	Approximate working time	Time to 70% of 7-day compressive strength
1%	20 min	4 hr
3%	16 min	4 hr
8.3%	7 min	2 hr

Cylinders from each batch of HCSC were tested at 7-days at ambient temperatures to assess batch-to-batch variability. Figure 3-1 shows the distribution of compressive strength. The results show that the compressive strength of the cast HCSC was roughly 9200 psi and was consistent, with low batch-to-batch variability.

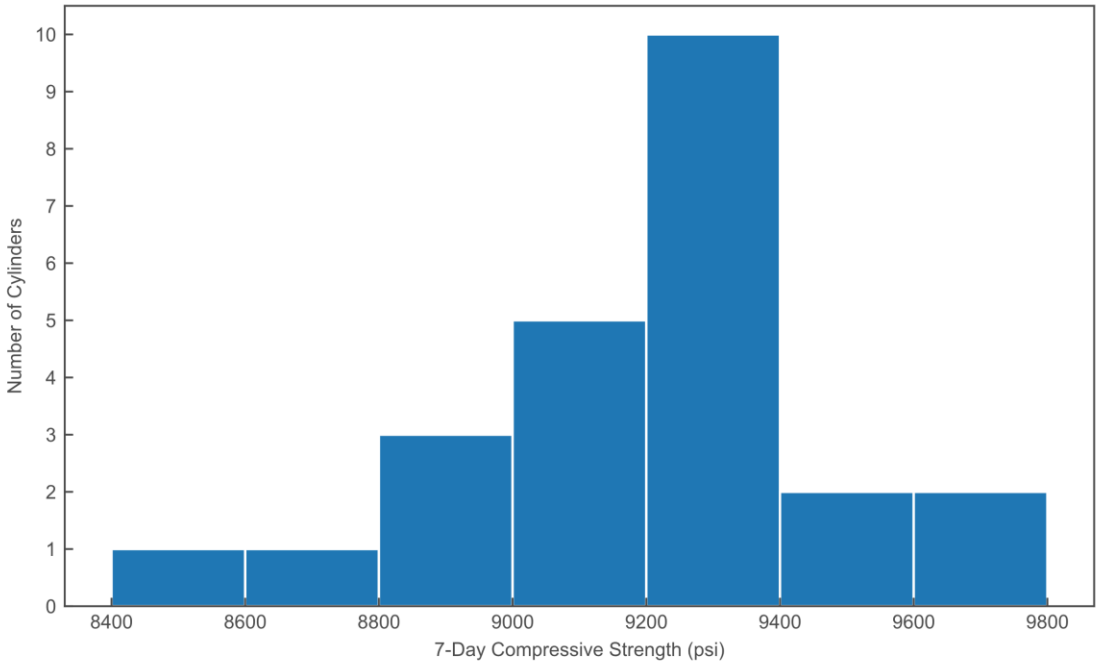

Figure 3-1. Histogram of 7-day compressive cylinder strengths

Figure 3-2 shows the exothermic behavior of cross-linking in HCSC during the curing process. Thermocouples were embedded in at least one specimen per batch to determine the temperature of specimens during conditioning and testing. Thermocouples were placed in the specimens such that they were in the center of the cross-section and would not disrupt the loading or impact the failure method. The peak temperature was between 105°F and 120 °F and varied between test samples

and batches. The temperature variation can be attributed to the variation in specimen size, and thus overall thermal mass, mold type and thickness, and ambient temperature.

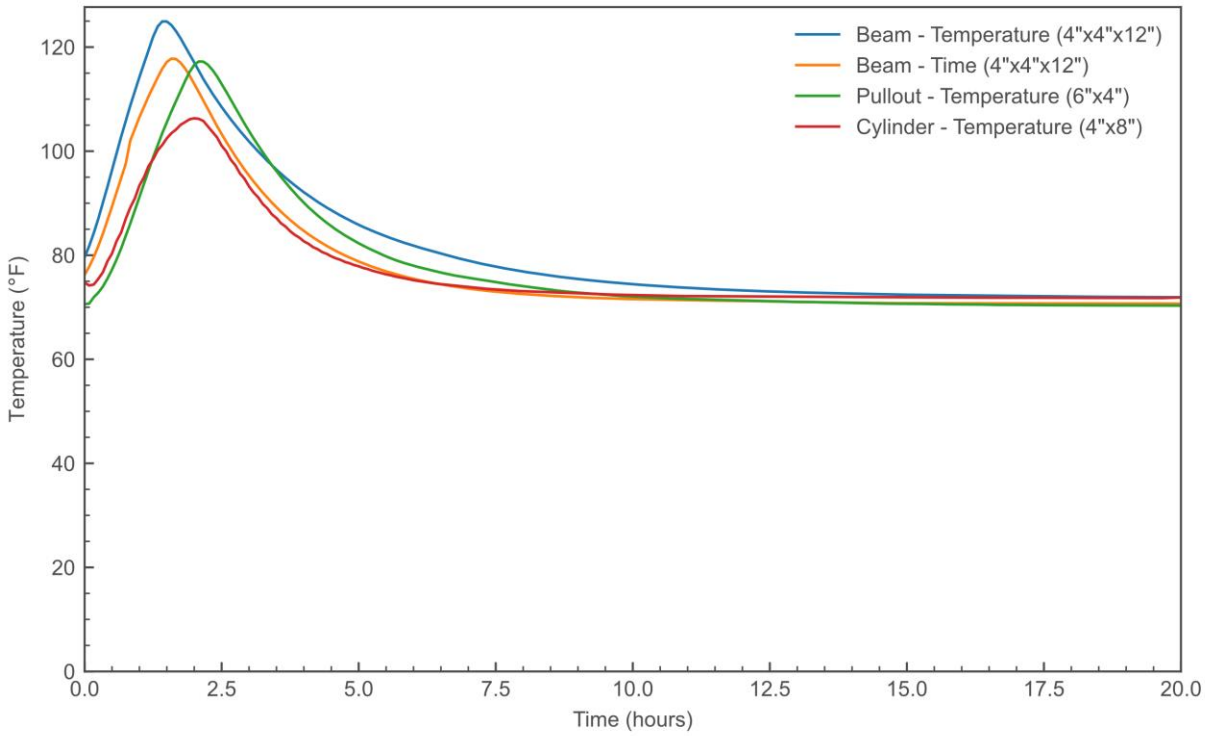

Figure 3-2. Temperature of specimens during curing

3.2. Mixing and Casting Procedure

Figure 3-3 shows the mixing procedure for the particular equipment used in this study. Each test batch (approximately 1.9 ft^3) was mixed in the laboratory using a standard drum mixer; however, in a field application, mixing would typically be completed using a volumetric mix truck to accommodate the required quantity of materials. The mixing procedure comprised four major steps:

1. If needed, mix HMWM per the manufacturer's recommended proportions and apply HMWM primer to the bond line and reinforcement. HCSC should be placed between 15-120 min after priming.
2. Mix HCSC resin with MEKP and Z-cure accelerator using a standard squirrel cage mixer until incorporation, around 45 seconds.
3. Add approximately 2/3rds of the resin mixture to the drum mixer then add approximately 2/3rds of the pre-package aggregate and fiber blend. Mix in the drum mixer until loosely incorporated.
4. Add in the remaining aggregate and fiber mix and the remainder of the resin blend. Mix for roughly two minutes.

Figure 3-3. (a) Mixing of MEKP and HCSC resin with a squirrel cage mixer, (b) Resin mixture being transferred from mixing bucket to drum mixing, (c) Adding the pre-packaged aggregate and fiber blend to the drum mixer, (d) HCSC mix turning in drum mixer, (e) HCSC placed in cylinder molds before finishing

Before mixing the HCSC, all formwork was prepared to help demold the HCSC after curing. Plastic molds were used for all cylinders, beams, and pullout specimens. Beam molds were sprayed with a release agent meant for casted polymers. Medium-density overlay (MDO) plywood was used as formwork for cementitious concrete casting, and melamine coated Medium-density fiberboard (MDF) was used for HCSC casting in non-contact splice specimens.

The following procedure was used to cast and cure the HCSC specimens:

1. Fill specimens in two lifts, consolidating the HCSC between lifts. The cylinders, beams, and bond pullout specimens were placed on a vibrating table for approximately 30 seconds per lift. The non-contact splice specimens were not externally or internally vibrated, but the corners and edges of the specimen were consolidated using small diameter rods .
2. Hand finish with a trowel.
3. For temperature conditioned specimen, cure for 24 hours at ambient temperatures

uncovered. For strength gain over time specimen, cure at ambient temperatures uncovered until testing time

5. Demold specimens. For temperature conditioned specimen, wait until 7-days post HCSC pour to begin conditioning or testing.

3.3. Test setup

Figure 3-4 shows the experimental setups and HCSC test specimens for the material characterization testing. The development of mechanical properties over time and the influence of temperature on the mechanical properties of cured HCSC were investigated by experimentally testing beam, cylinder, and bond specimens under monotonic loads to failure.

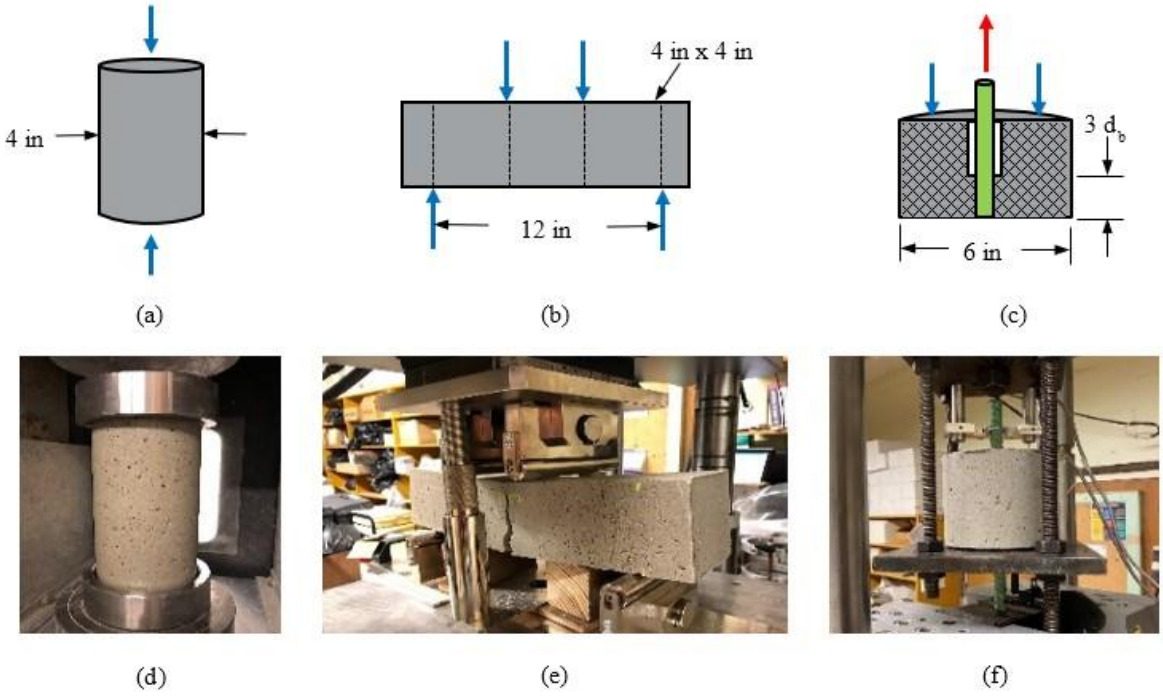

Figure 3-4. Diagrams and test setup for (a/d) compressive strength, (b/e) modulus of rupture, (c/f) bond pullout

Compressive strength tests were conducted according to ASTM C39 (ASTM 2021a). Flexural strength tests were conducted according to ASTM C78 (ASTM 2021b). Pullout bond cylinders were tested following the procedures of ASTM D7913 (ASTM 2020a), however, the specimen size was reduced and epoxy-coated reinforcement was used. Given the higher tensile strength of HCSC in comparison to conventional concrete that is used in the ASTM D7913 standard, this reduction was deemed appropriate. This provided a measure of the pure bond strength when failure occurred by reinforcement pullout, which was later used in determining the experimental design parameters for non-contact splice testing. The testing procedure used was similar to that of Peruchini et al. (2017) who tested bond pullout cylinders with UHPC.

Figure 3 3a shows the pullout bond cylinder specimens under construction. An epoxy-coated #5 rebar was cast in the center of a 6 in diameter by 6 in tall cylinder mold. The bottom four inches of the rebar were debonded from the HCSC by placing a PVC tube around the rebar and sealing

the top and bottom. This resulted in a two-inch bonded length and ensured a pullout failure mode instead of splitting of the polymer concrete. Figure 3-5b and Figure 3-5c show the test configuration. The specimens were suspended by the bottom face (closest to the debonded section) via a steel plate with a hole in the middle, and the bottom portion of the rebar was gripped by the testing machine. Two LVDTs, oriented at 180 degrees from each other, were placed four inches above the hand-finished top face of the specimen to record the pullout of the reinforcement relative to the top (back) face of the cylinder.

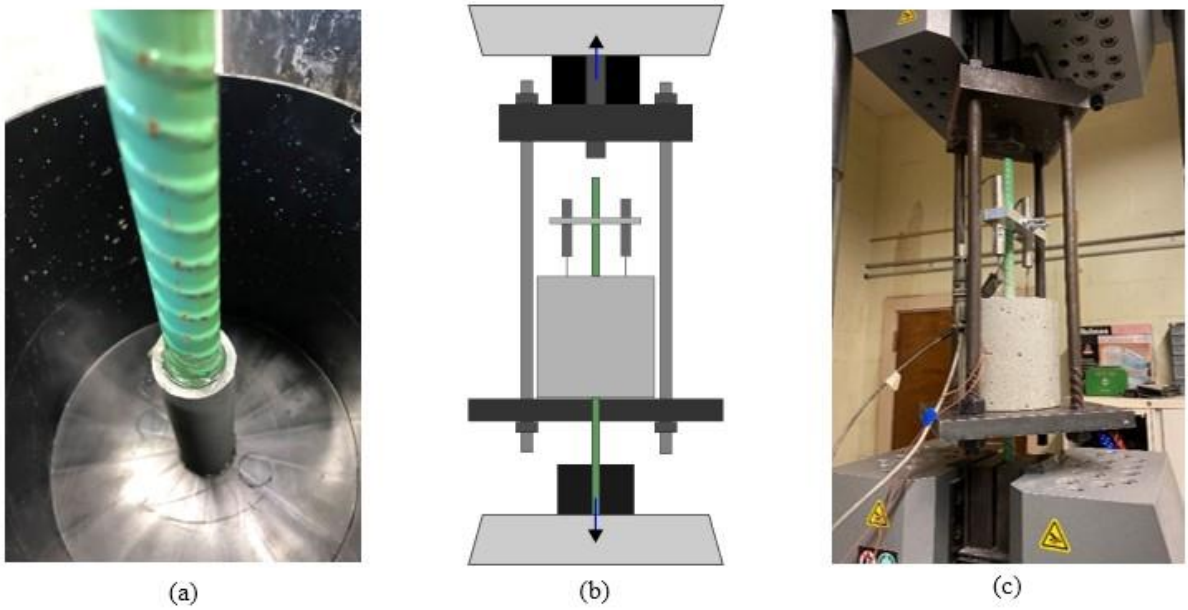

Figure 3-5. Bond pullout test specimens and test setup (a) Debonded section of the reinforcement, (b) test diagram, (c) test setup

For each strength test, two batches of HCSC specimens were cast. One batch of specimens was tested at various temperatures and one batch was tested at various times throughout the curing process. Table 3-4 shows the approximate intervals and number of specimens tested for each strength test. For each batch of specimens, the 7-day compressive strength of the HCSC was also determined and used as a control test to ensure consistent batching, mixing, and curing of the HCSC throughout the testing program.

Table 3-4. Mechanical property specimen catalog

Test Type	Parameter	Approximate Interval	Number of Specimens
Compression	Time-Strength (hrs) Temperature (°F)	2, 2.5, 3, 3.5, 4, 5, 6, 7, 8 10, 45, 80, 115	1 per time plus 3 at 7 days, 12 total 3 per temperature, 12 total
Flexure	Time-Strength (hrs) Temperature (°F)	2, 3, 4 ,5 ,6 ,8 ,12, 24, 72 10, 45, 80, 115	1 per time plus 3 at 7 days, 12 total 3 per temperature, 12 total

Test Type	Parameter	Approximate Interval	Number of Specimens
Bond Pull	Time-Strength (hrs) Temperature (°F)	2, 2.5, 3, 4, 6, 8, 12, 24, 72 10, 45, 80, 115	1 per time plus 3 at 7 days, 12 total 3 per temperature, 12 total

3.4. Strength Gain Over Time

To quantify the evolution of mechanical properties over time, especially the strength gain over the first few hours after mixing, test specimens (cylinders, beams, bar pulls) were cast and allowed to cure under ambient conditions (roughly 75 °F and 45% RH). Starting at the earliest feasible time (determined to be 2 hours after mixing), specimens were removed from their molds and tested to failure at least every hour, until 8 hours after mixing. The remaining specimens were tested at convenient intervals, and three specimens were reserved for testing at 7 days.

Figure 3-6 shows the complete stress-strain relationship for HCSC at different ages, established under displacement control at a rate of 0.05 in/min. The strengths and elastic moduli were both somewhat lower (between 5-10%) than those obtained under load control, loaded at 20 to 50 psi/sec consistent with ASTM C39 [ASTM 2021].

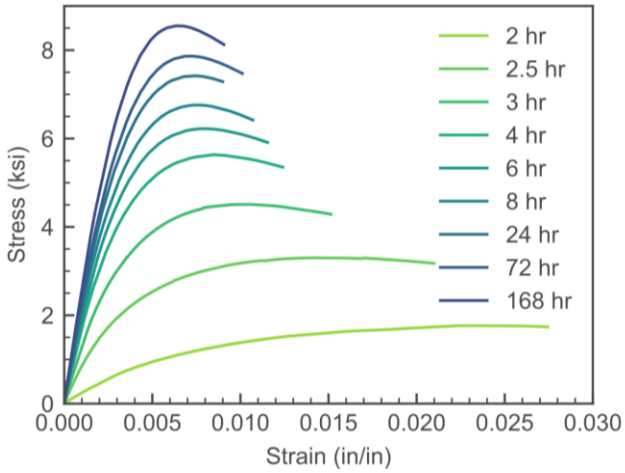

Figure 3-6. Compressive stress-strain behavior of HCSC as a function of time

Figure 3-7 shows the mechanical properties of HCSC as a function of time after mixing. The bond strength reported here is the peak average bond stress recorded during the test. The 7-day values are also shown in the plots as horizontal dashed lines, as are the 14-day material properties of non-proprietary UHPC tested by Peruchini et al. 2017. Overall, the development of mechanical properties was consistent between the four test series, with a majority of the strength and modulus development occurring over the first 8 hours after mixing. The development of flexural strength occurred sooner than the development of the compressive strength or bond, although the three curves are very similar. This is consistent with observations made by others for cementitious concretes (e.g., Peruchini et al. 2017) although the behavior is seen here on a scale of hours rather than days. By 4 hours after mixing, the compressive, flexural, and bond strengths were 70%, 80%, and 75% of their 7-day values, respectively. This would likely be sufficient to allow opening of the bridge being built or reopening of a repair to traffic.

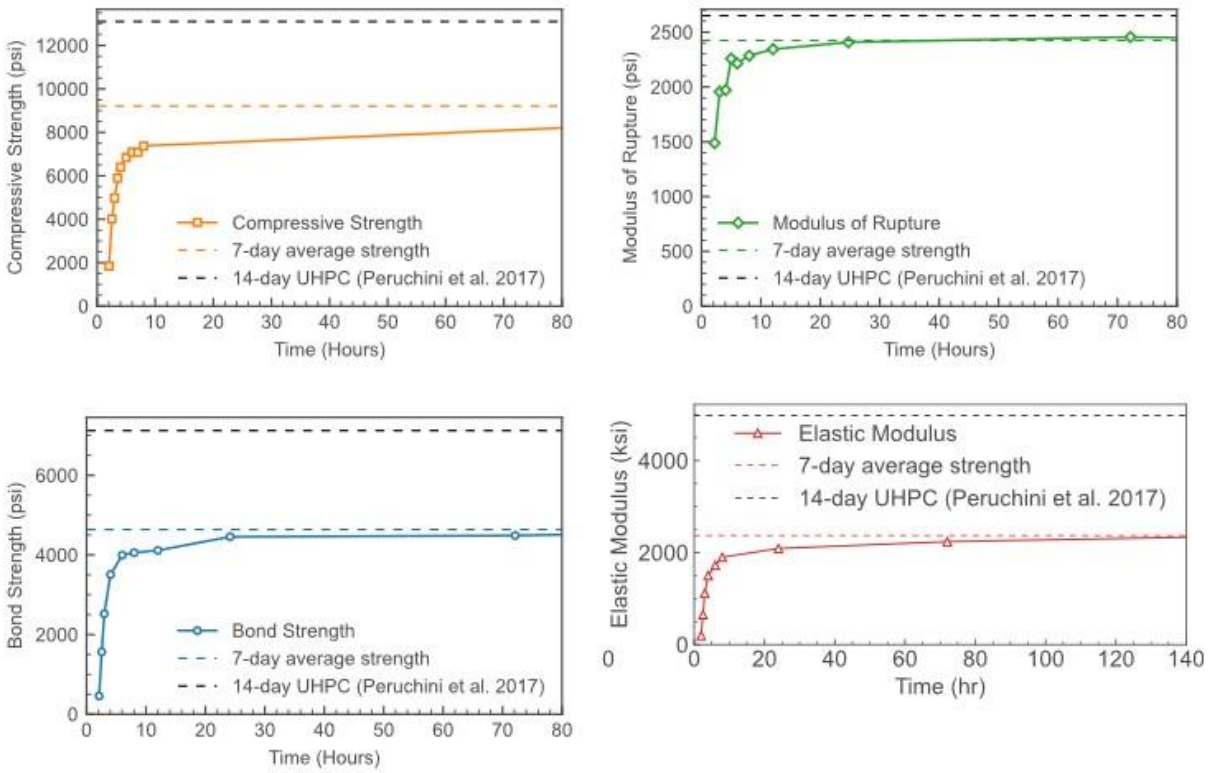

Figure 3-7. Mechanical properties (compression, flexure, bond, modulus) as a function time after mixing

Fig 3-8 shows the average bond stress with respect to the back-end slip of the reinforcement as a function of time The average bond stress was computed by dividing the measured load by the notional surface area of the bar, idealized as a smooth cylinder with diameter equal to the nominal value, that was in contact with the FRPC. As the bond stress increased initially, there was minimal slip. Once the maximum bond stress was reached, the curves softened with diminished bond stress and increasing slip. At large values of slip (e.g., 0.2 in) some residual bond stress remained due to friction between the reinforcement and the concrete. As the HCSC continued to cure, the maximum bar stress increased with decreasing amounts of slip before peak bar stress. For all tests except the 7-day test, the yield stress of the reinforcing was not reached.

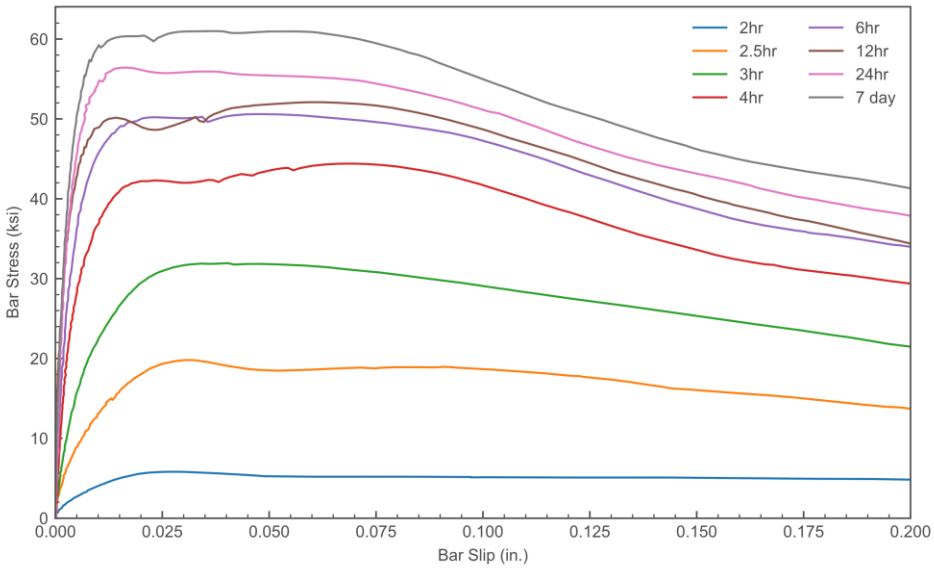

Figure 3-8. Stress- back-end slip for bond pullout testing as a function of time after mixing

3.5. Influence of Testing Temperature

To elucidate the influence of temperature on the mechanical properties of HCSC, test specimens (cylinders, beams, bar pulls) were cast and allowed to cure under ambient conditions (roughly 75 °F and 45% RH) for 7 days. The specimens were then conditioned to the target test temperatures (10 °F, 45 °F, 115 °F) using temperature-controlled cabinets. The specimens were kept in the temperature-controlled cabinets for at least 16 hours prior to testing to achieve the desired internal temperature, monitored by embedded thermocouples in select specimens. The specimens were then removed, one by one, from the cabinets and tested promptly. The surface temperature of the specimens was recorded before and after each test. Three specimens per temperature were tested. A set of specimens were also tested under ambient conditions at 7 days for reference.

Figure 3-9 shows the complete stress-strain relationship for HCSC at four temperatures, established under displacement control at a rate of 0.05 in/min. The stress strain curves for the cylinders tested at 5 °F were limited by the capacity of the universal testing machine. The strengths and elastic moduli were both somewhat lower (between 5-10%) than those obtained under load control, loaded at 20 to 50 psi/sec consistent with ASTM C39 [ASTM 2021]. At elevated temperatures, the material was more flexible and less strong, compared to its properties at cooler temperatures.

Figure 3-10 shows the mechanical properties of FRPC as a function of temperature over the range of temperatures tested. Three specimens per temperature were tested, and a set of specimens were also tested under ambient conditions at 7 days for reference. The bond strength reported here is the peak average bond stress recorded during the test. The temperature shown in the figure is the surface temperature of the sample at the start of testing. Deviation from the target temperature was evident in the data, due to changes in specimen temperature during handling and setup. Overall, the variation of mechanical properties was consistent between the four test series, with an increase in strength and modulus observed for specimens conditioned to colder than room temperature and

a decrease observed for specimens conditioned to above room temperature. The relationship between strength and temperature was roughly linear.

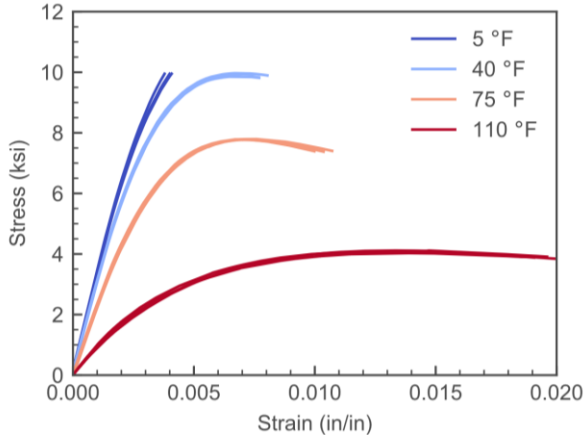

Figure 3-9. Compressive stress-strain behavior of HCSC as a function of temperature (5 °F curve limited by the capacity of the testing machine)

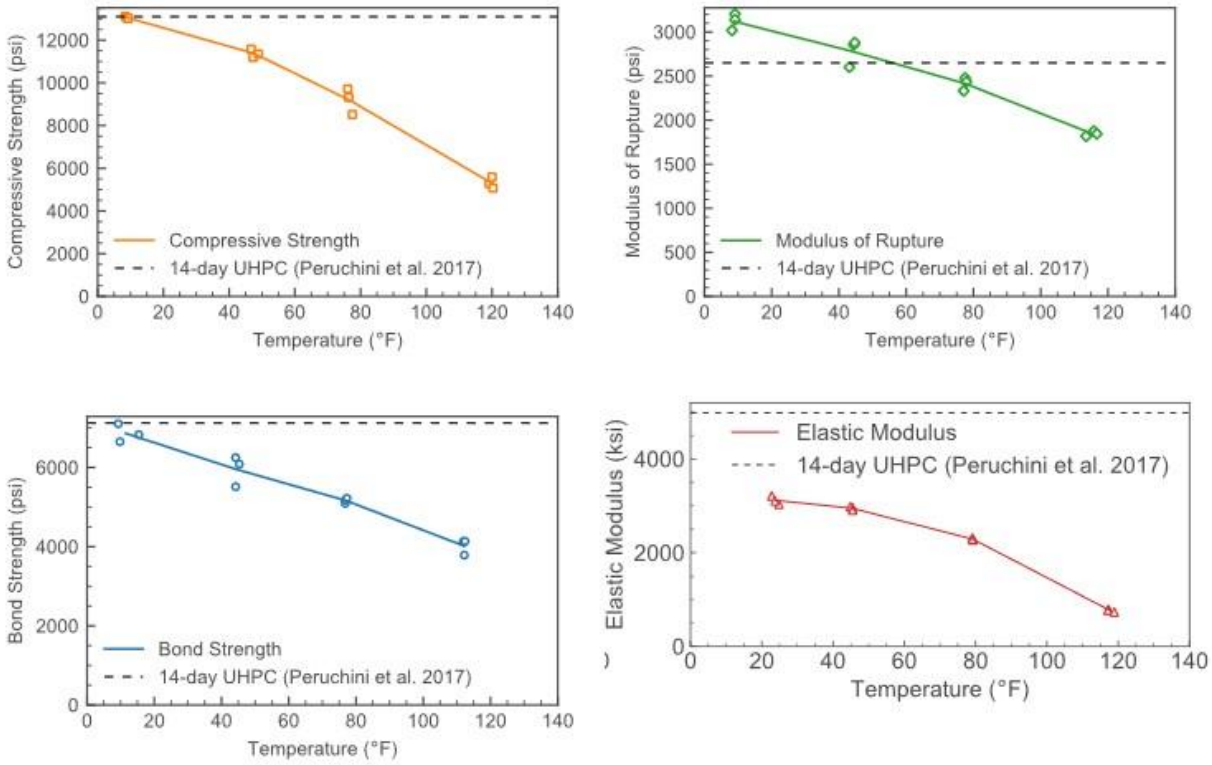

Figure 3-10. Mechanical properties (compression, flexure, bond) as a function of test temperature

Figure 3-11 shows the influence of testing temperature on the normalized strengths (compression, flexure, and bond) of the samples, along with a regression line of the entire dataset. The normalized strength was calculated by dividing the strength data by the corresponding average ambient temperature value, used here to enable comparison between the three different strengths. A temperature change of 40 °F resulted in a roughly 25% change in material strength, a significant variation that must be accounted for in design. For a unit change of 1 °F, there is a change of 0.6% of the normalized strength.

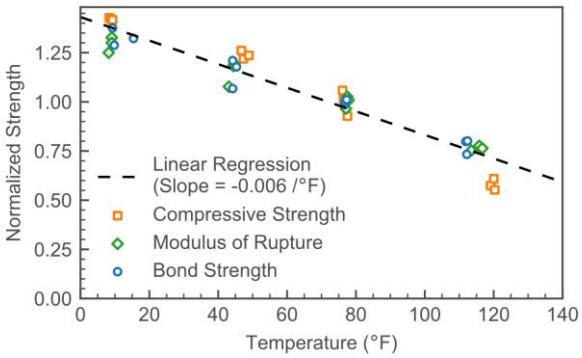

Figure 3-11. Linear Strength Regression (normalized) as a function of test temperature

Figure 3-12 shows the bar stress with respect to the back end slip of the reinforcement. The general stress-slip behavior is similar to Figure 3-8. For lower temperatures, there is less slip during the initial phase of loading before maximum bar stress than compared to warmer temperatures. For specimens tested at room temperature and colder, bar yield was reached. As the testing temperature decreases a plateau appears around the peak bar stress as the back end slip increases with little change in the bar stress. This behavior is similar to that of well-confined concrete. This can be attributed to the high material strengths and resistance to splitting at lower testing temperatures. As the testing temperature decreased, the bond stress increased for all levels of back-end slip. At lower temperatures (e.g. 43 °F), there was less slip during the initial phase of loading before maximum bond stress than compared to warmer temperatures (e.g. 116 °F). Although only a short bonded length (3 d_b) was provided, in order to promote bond failure before bar yielding, the specimens tested at below room temperature achieved bar stresses above the measured yield stress (64.5 ksi).

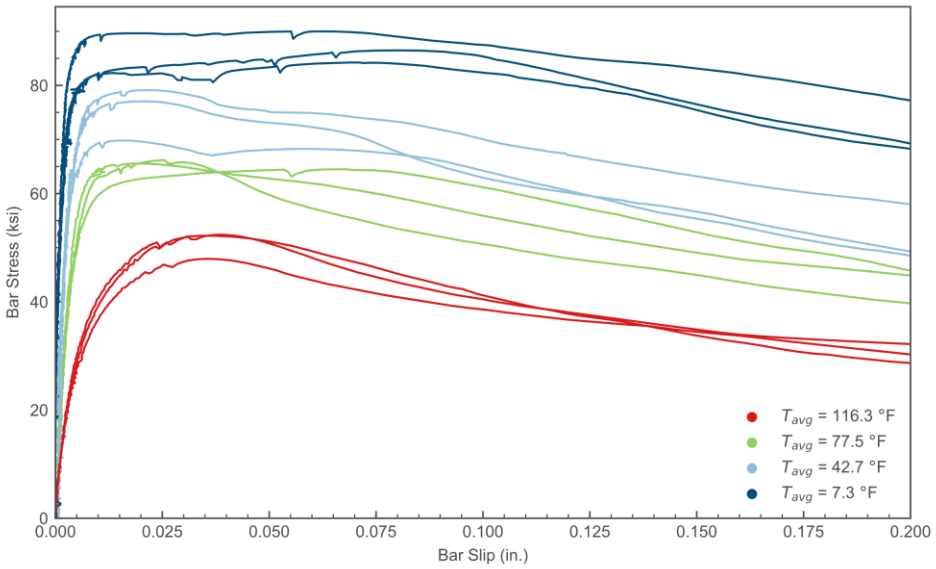

Figure 3-12. Stress- back-end slip for bond pullout testing as a function of testing temperature

CHAPTER 4. NON-CONTACT SPLICE TESTING PROGRAM

To characterize the effects of various parameters on bond, non-contact splice tests were performed on epoxy-coated deformed bars embedded in FRPC. The tests focused on a simplified, non-contact splice configuration that isolated the behavior of the reinforcement in a closure joint. The test setup and parameters were similar to previous studies by Qiao et al. (2016) for testing non-contact splices embedded in UHPC. Yuan and Graybeal (2014) also conducted pullout tests to evaluate the factors that affect bond strength between deformed reinforcing and UHPC. The pullout tests performed by Yuan and Graybeal were the first to investigate UHPC as a closure joint material. Many other studies following the initial research have also used a version of this setup. The test setup used by Yuan and Graybeal is shown below, Figure 4-1.

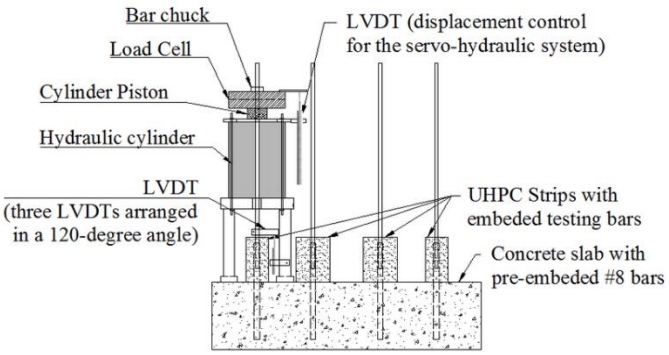

Figure 4-1. Loading setup by Yuan and Graybeal (2014)

4.1. Experiment Design

Table 4-1 and Table 4-2 show the non-contact splice test matrix. The experimental matrix for this test series was constructed as a rotatable central composite design (CCD) (Box et al. 2005), with the varied parameters being test temperature, T; splice length, ℓ_s; side cover, c_b; and bar diameter, d_b. The CCD design included an embedded factorial design, repeated center points to quantify batch-to-batch uncertainty, and additional axial points that allowed for the estimation of curvature in the region of interest. The experimental design was centered around the point (T =75 °F, ℓ_s = 3.75 in, c_b = 2.0 in, and d_b = 0.625 in) in the parameter space. The tests were conducted in three sets, or "blocks", comprising 10 specimens apiece. Each block of specimens was made from the same batch of HCSC.

Table 4-1. Summary of test parameters

Bar size	Temperature (°F)	Side Cover (in.)	Overlap length (in)
No. 3	5 °F	0.75	1.25
No. 4	40 °F*	1.375*	2.5*
No. 5*	75 °F*	2*	3.75*
No. 6	110 °F*	2.625*	5*
No. 7	145 °F	3.25	6.25

*Parameters used in scoping study (Batch 0)

The parameters chosen for non-contact splice testing encompass typical values for closure pours in western Washington and many other parts of the United States.

- Bar size was centered around No. 5 bars, typical for the deck reinforcement of prefabricated superstructure components. In all tests, bar spacing of the uncoated bars was held constant at 6 in, center-to-center.
- Test temperatures encompass summer highs and winter lows in western Washington centered around a temperature that is slightly above standard room temperature (75 °F). Tests were completed at ambient lab temperatures.
- Bar cover, expressed here as the distance from the edge of the specimen to the center of the reinforcement, is consistent with tests performed by Peruchini et al. (2017), Qiao et al. (2016), and Yuan and Graybeal (2014).
- The overlap length or splice length is based on the calculated embedded lengths for reinforcement yield and fracture from the mechanical characterization findings. Based on the data, the embedded length required to yield a No. 5 epoxy-coated bar varied from 1.5 in. to 2.6 in. for the range of temperatures tested. The embedded length needed to fracture a No. 5 bar varied from 2.2 in. to 3.8 in. The overlap length used here is necessarily longer, accounting for differing test configurations, the spacing between bars in the non-contact splice, and the reduction in side cover.

Table 4-2. Non-contact splice experimental matrix

Block/ Batch	Run	Temperature T (°F)	Splice length ℓ_s (in)	Side Cover c_b (in)	Bar diameter d_b (in)	Point Description
1	1-01	40	5	1.375	0.5	Factorial
1	1-02	40	2.5	2.625	0.5	Factorial
1	1-03	110	2.5	1.375	0.5	Factorial
1	1-04	110	5	2.625	0.5	Factorial
1	1-05	40	2.5	1.375	0.75	Factorial
1	1-06	40	5	2.625	0.75	Factorial
1	1-07	110	5	1.375	0.75	Factorial
1	1-08	110	2.5	2.625	0.75	Factorial
1	1-09	75	3.75	2	0.625	Center
1	1-10	75	3.75	2	0.625	Center
2	2-01	40	2.5	1.375	0.5	Factorial
2	2-02	40	5	2.625	0.5	Factorial
2	2-03	110	5	1.375	0.5	Factorial
2	2-04	110	2.5	2.625	0.5	Factorial
2	2-05	40	5	1.375	0.75	Factorial
2	2-06	40	2.5	2.625	0.75	Factorial
2	2-07	110	2.5	1.375	0.75	Factorial
2	2-08	110	5	2.625	0.75	Factorial
2	2-09	75	3.75	2	0.625	Center
2	2-10	75	3.75	2	0.625	Center
3	3-01	75	3.75	2	***0.375***	Axial

Block/ Batch	Run	Temperature T (°F)	Splice length ℓ_s (in)	Side Cover c_b (in)	Bar diameter d_b (in)	Point Description
3	3-02	75	3.75	2	***0.875***	Axial
3	3-03	***5***	3.75	2	0.625	Axial
3	3-04	***145***	3.75	2	0.625	Axial
3	3-05	75	3.75	**0.75**	0.625	Axial
3	3-06	75	3.75	**3.25**	0.625	Axial
3	3-07	75	***1.25***	2	0.625	Axial
3	3-08	75	***6.25***	2	0.625	Axial
3	3-09	75	3.75	2	0.625	Center
3	3-10	75	3.75	2	0.625	Center

An additional scoping study (block zero), Table 4-3 was added to characterize the effects of the use of the HMWM primer at the bond line and between the reinforcement and concrete. These additional tests assessed if primer could be omitted in the larger test series and the results could support less stringent requirements when access and schedule make the application of primer impractical. A fractional factorial design (2^{3-1} – Resolution III) was used. Five specimens were cast without the HMWM primer along with five specimens with identical parameters with HMWM applied per manufacturer instructions.

Table 4-3. Scoping study experimental matrix

Block/ Batch	Run	Temperature T (°F)	Splice length ℓ_s (in)	Side Cover c_b (in)	Bar diameter d_b (in)	Point Description
0	0-01p	110	2.5	1.375	0.625	Primer
0	0-01	110	2.5	1.375	0.625	No primer
0	0-02p	40	2.5	2.625	0.625	Primer
0	0-02	40	2.5	2.625	0.625	No primer
0	0-03p	40	5	1.375	0.625	Primer
0	0-03	40	5	1.375	0.625	No primer
0	0-04p	110	5	2.625	0.625	Primer
0	0-04	110	5	2.625	0.625	No primer
0	0-05p	75	3.75	2	0.625	Primer
0	0-05	75	3.75	2	0.625	No primer

4.2. Specimen Geometry

Figure 4-2a shows the specimen geometry that was used in this project. Specimens were sized such that they could be conditioned to different test temperatures using conventional laboratory equipment and tested using a universal testing machine under precise displacement control. Figure 4-2b shows the test configuration that was used for the tests, which was similar to the configuration used by Qiao et al. (2016). The use of a full-width precast slab, similar to Yuan and Graybeal (2014) shown in Figure 4-1, would have increased the test complexity and cost and has not been shown to significantly influence the performance of non-contact splice specimens in previous

studies (Graybeal and Yuan 2014, Haber and Graybeal 2018); neither concrete damage in the precast slabs nor tension failure between the UHPC strip and the precast concrete were reported during either of these test series. Instead, steel fixtures were used to anchor the reinforcement instead of a slab. A precast concrete "strip" between anchor bars, roughly equal in size to the FRPC strip and below the splice was used to stiffen the specimen. An exposed aggregate roughened surface was provided on the precast concrete strip, the surface was primed using HMWM, and HCSC was cast against it in the horizontal position, mimicking the field orientation of the joint.

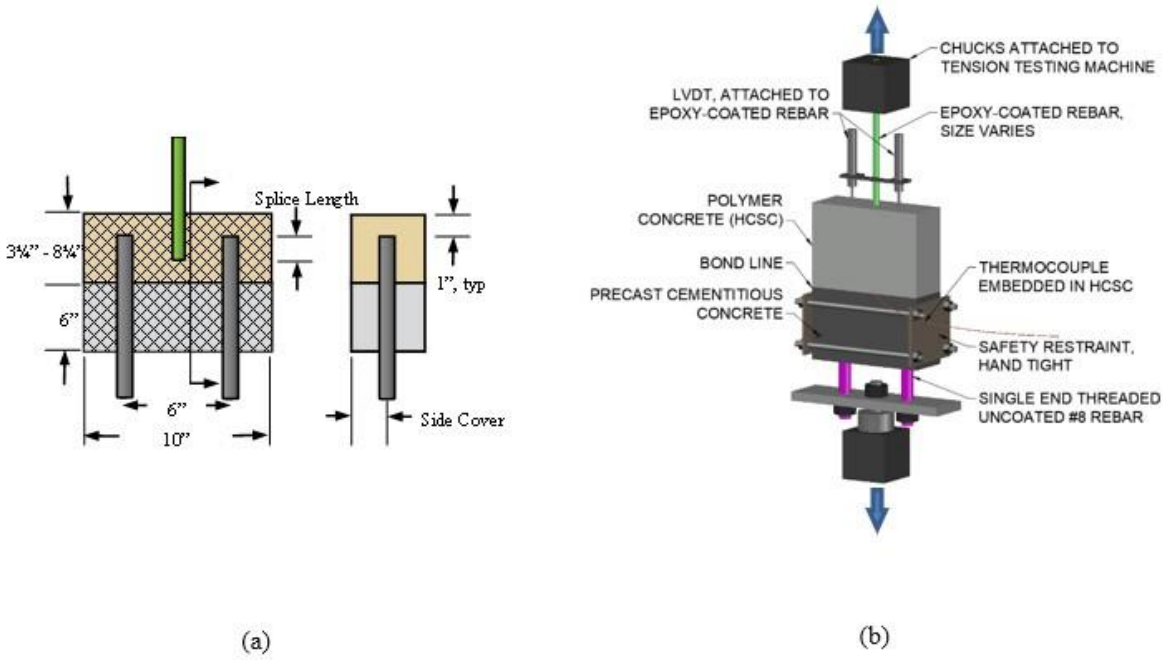

Figure 4-2. Contact splice specimens (a) section and elevation and (b) test setup

4.3. Materials

The cementitious concrete used as the stiffening strip for each specimen had a maximum aggregate size of 3/8 in. One batch of concrete was mixed per testing block. Compressive strength testing was completed 28 days after casting, and the average 28-day compressive strength of the concrete was 4500 psi.

Figure 4-3 shows the reinforcement stress-strain curves for each bar size used in the experimental program. Table 4-4 summarizes the average yield and tensile strengths for each bar designation. All reinforcing used in the material testing and non-contact splice testing were normal strength Grade 60 uncoated and epoxy-coated reinforcement. The reinforcement met ASTM A706 (ASTM 2022), with the coating meeting ASTM A775 (ASTM 2019). All bars were tested following ASTM A370 (ASTM 2020b). Two to four bars were tested for each bar size using an extensometer with a 2 in gage length under displacement control. The yield strength for each test was determined using the 0.2% offset method.

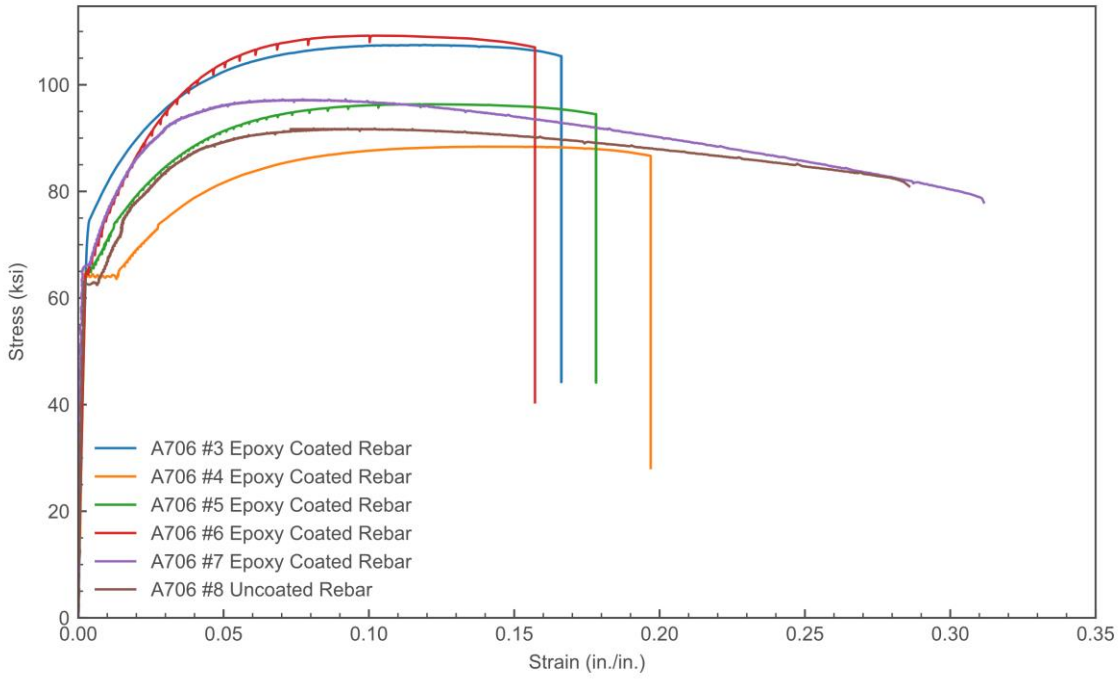

Figure 4-3. Tensile stress-strain response of epoxy-coated reinforcing bars

Table 4-4. Properties of reinforcing steel

Bar Size	Avg Yield Strength (psi)	Avg Tensile Strength (psi)
No. 3*	74900	107400
No. 4*	64800	89000
No. 5*	64500	96000
No. 6*	66400	109200
No. 7*	66600	97400
No. 8	66900	92700

* Epoxy coated reinforcement meeting ASTM A775

Table 4-5 shows the compressive strengths of each batch of HCSC used in the non-contact splice specimens. Compressive strength testing was completed at the midpoint of testing for each group of temperatures for each batch. Three compressive cylinders were tested for each batch at each temperature. The same HCSC mix ratios used in the mechanical characterization testing were used for the non-contact splice tests. All blocks were cast with a single batch of HCSC, with approximately 230 lbs of prebagged aggregate and basalt fiber mix. The same mixing and casting procedure was used for the non-contact splice specimens, as described in Section 3.2, with HMWM primer being applied as described in Section 3.2.

Table 4-5. HCSC compressive strengths

Type	Block #	Age of specimen (days)	Average Temperature (°F)	Average Compressive Strength (psi)
Room	0	7	71.4	9395
Room	1	12	71.4	9241
Room	2	12	71.0	9591

Type	Block #	Age of specimen (days)	Average Temperature (°F)	Average Compressive Strength (psi)
Room	3	7	75.3	9250
Hot	0	18	120.4	5600
Hot	1	13	116.1	5681
Hot	2	14	117.7	5245
Hot	3	11	157.7	1756
Cold	0	18	41.2	11664
Cold	1	14	23.6	13002
Cold	2	17	37.7	11883
Cold	3	11	11.7	12724

4.4. Specimen Construction and Conditioning

Non-contact splice specimens were constructed in two steps. First, the lower, precast concrete block was constructed by passing uncoated rebar, threaded at one end, through MDO plywood forms (Figure 4-4a and Figure 4-4b). The future bond line between the cementitious concrete and polymer concrete was prepared using a paint-on form retarder for an exposed aggregate finish (Figure 4-4c) and the concrete was mixed and cast following standard laboratory practices. Second, after the cementitious concrete cured for 7 days, melamine coated MDF forms were constructed around the precast concrete blocks (Figure 4-4d) and the mixing and fabrication procedure outlined in Section 3.2 were followed to cast the remaining portion of the specimen, containing the HCSC.

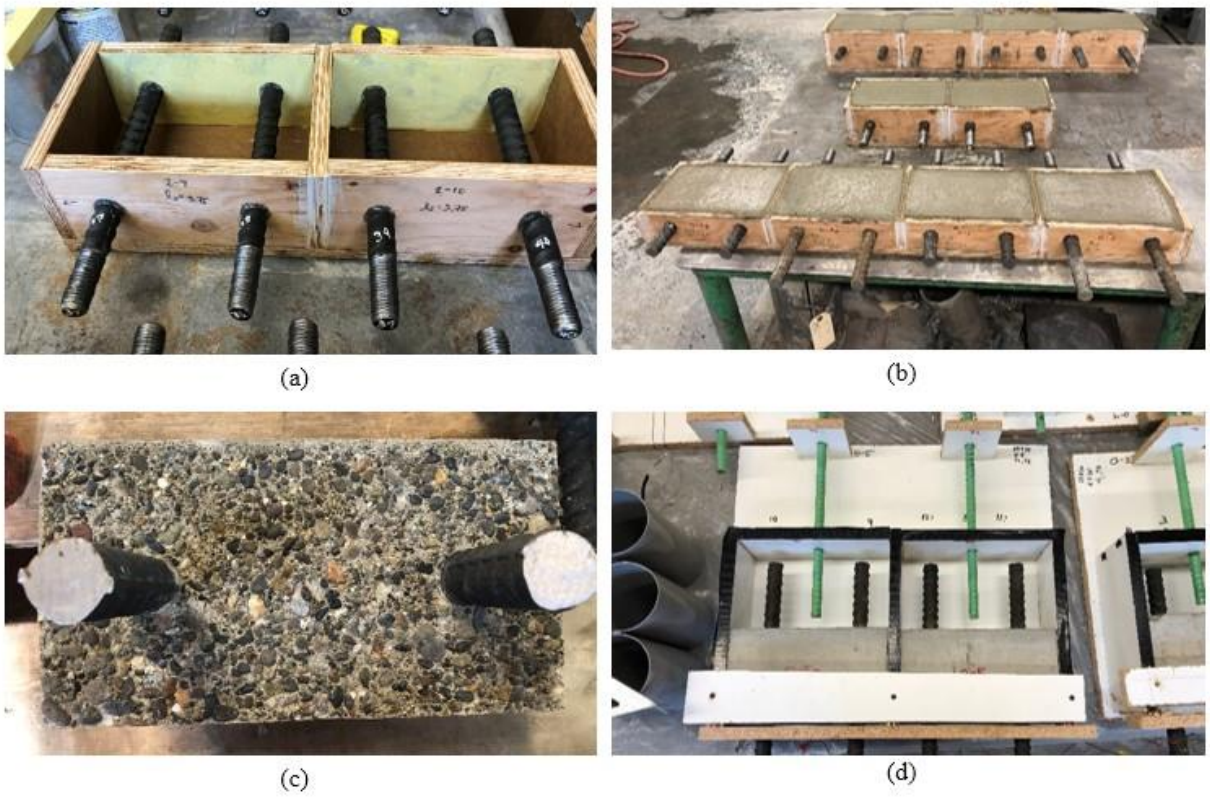

Figure 4-4. Non-contact splice specimen casting procedure: (a) cementitious concrete formwork, (b) cast cementitious concrete, (c) exposed aggregate finish, (d) HCSC formwork

Once demolded and cured for 7 days under ambient conditions, the specimens were conditioned to the target test temperatures. The specimens were kept in the temperature-controlled cabinets for at least 16 hours prior to testing to achieve the desired internal temperature, monitored by embedded thermocouples in the specimens. Figure 4-5 shows the internal temperature change for non-contact splice specimens during the conditioning period. The dashed lines indicate the temperature of the chamber.

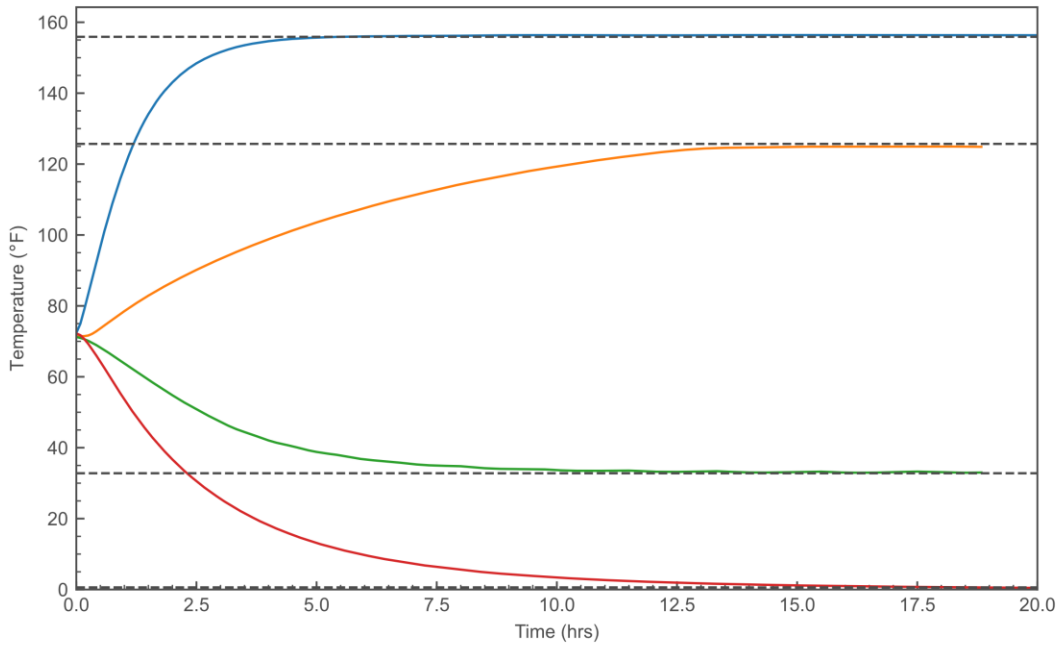

Figure 4-5. Temperature of non-contact splice specimens during conditioning

4.5. Instrumentation

Figure 4-6 shows the instrumentation that was applied to non-contact splice specimens. The tests were conducted using a 600 kN Instron Universal Testing Machine (UTM), which recorded the applied load and crosshead displacement during testing. In addition to these integral measurements, LVDTs arranged at 180 degrees to each other were attached to the epoxy-coated rebar 4 in above the top face of the specimen to record the slip displacement of the reinforcement relative to the top face of the HCSC and Type J thermocouples were embedded in the HCSC portion of the specimen, at approximate mid-depth, in order to monitor the internal temperature of specimens during the casting, curing, and testing process. Data was recorded at five-minute intervals during the casting and curing process and at 10 Hz during testing. An additional thermocouple was kept exposed to record the ambient temperature of the laboratory and an additional LVDT recorded the movement of the UTM crosshead, which allowed the LVDT and thermocouple measurements to be synchronized with the UTM load and displacement.

(a) (b)

Figure 4-6. (a) LVDT placement on reinforcement, (b) embedded thermocouples

4.6. Test Setup and Procedure

Figure 4-7 shows the test setup for the non-contact splice specimens. Testing was conducted by applying monotonically increasing vertical displacements to the free ends of the reinforcement and measuring the resulting loads using the test machine's internal load cell. The two No. 8 anchorage bars were threaded at their ends and were used to connect the specimens to the bottom platen of the testing machine, which remained fixed. The free end of the epoxy-coated reinforcement was gripped in the top jaws of the testing machine. The tension load was applied under closed-loop displacement control at a constant rate of 0.2 in./min. To prevent damage to the instrumentation and test machine when the specimen failed, the concrete strip was restrained transverse to the axis of the splice using exterior steel plates and four 0.5 in diameter threaded rods. The rods were snugged tight by hand before starting the tests, providing minimal restraint against splitting at the top surface of the specimen.

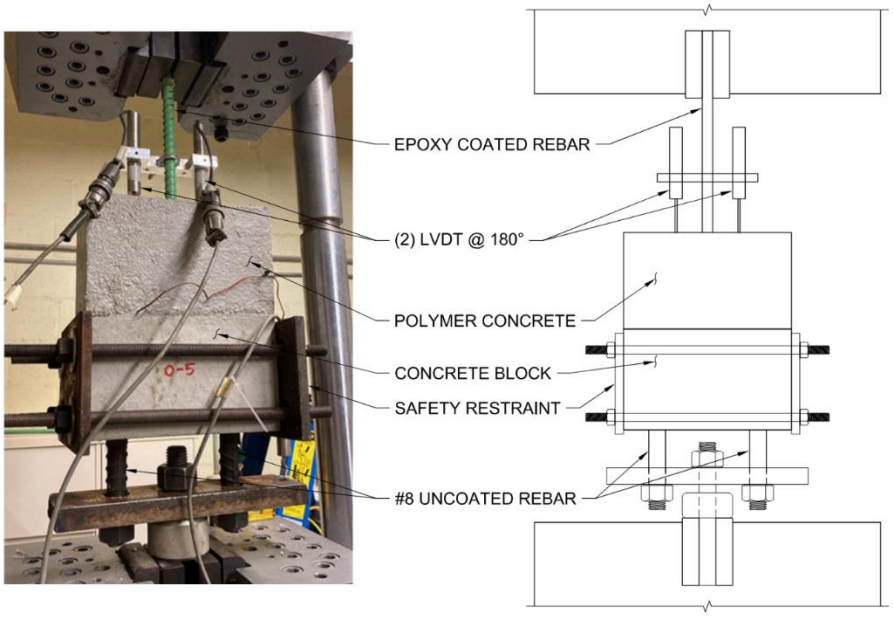

Figure 4-7. Non-contact splice testing setup

Table 4-6 shows the average surface and internal temperature for each testing temperature. During testing, the specimens were individually removed from the conditioning chamber and promptly tested to reduce deviation from the target test temperatures. While the testing duration varied between tests, a larger temperature change was observed for specimens tested at low temperatures, indicating different rates of heat flow.

Table 4-6. Average surface and average internal temperatures (°F) during testing

Target Temp (°F)	Avg Surface Temp Start	Avg Surface Temp End	Avg Internal Temp Start	Avg Internal Temp End
40 (n = 8)	44.0	46.5	30.4	32.0
110 (n = 8)	116.6	115.6	118.6	118.0
5 (n = 1)	14.7	17.4	1.4	4.0
145 (n = 1)	155.8	151.8	155.7	153.6

Because the expected failure mode of the specimens was bond-splitting, the temperature of the HCSC at the front end of the reinforcement was most critical, and therefore the surface temperature was used when comparing test results.

CHAPTER 5. EXPERIMENTAL RESULTS

Table 5-1 summarizes the results of the non-contact splice tests for the scoping study and CCD design.

Table 5-1. Summary of experimental testing results

Block/ Batch	Run	Point Description	Observed Failure	Max Load (lb)	Bar Stress (ksi)
0	0-01p	Primer	Splitting	12419	40.06
0	0-01	No primer	Splitting	11136	35.92
0	0-02p	Primer	Splitting	25086	80.92
0	0-02	No primer	Splitting	22760	73.42
0	0-03p	Primer	Splitting	23071	74.42
0	0-03	No primer	Splitting	19844	64.01
0	0-04p	Primer	Splitting	26157	84.38
0	0-04	No primer	Splitting	25722	82.97
0	0-05p	Primer	Splitting	24524	79.11
0	0-05	No primer	Splitting	22313	71.98
1	1-01	Factorial	**Bar Fracture**	17433	87.17
1	1-02	Factorial	**Bar Fracture**	17494	87.47
1	1-03	Factorial	Splitting	12103	60.52
1	1-04	Factorial	**Bar Fracture**	17082	85.41
1	1-05	Factorial	Splitting	17225	39.15
1	1-06	Factorial	Splitting	42262	96.05
1	1-07	Factorial	Splitting	21422	48.69
1	1-08	Factorial	Splitting	19222	43.69
1	1-09	Center	Splitting	26561	85.68
1	1-10	Center	Splitting	25625	82.66
2	2-01	Factorial	Splitting	14655	73.28
2	2-02	Factorial	**Bar Fracture**	17426	87.13
2	2-03	Factorial	Splitting	15201	76.01
2	2-04	Factorial	**Pullout**	14159	70.80
2	2-05	Factorial	Splitting	24165	54.92
2	2-06	Factorial	Splitting	29765	67.65
2	2-07	Factorial	Splitting	13765	31.28
2	2-08	Factorial	Splitting	30539	69.41
2	2-09	Center	Splitting	24481	78.97
2	2-10	Center	Splitting	25245	81.44
3	3-01	Axial	**Bar Fracture**	11443	104.03
3	3-02	Axial	Splitting	30437	50.73
3	3-03	Axial	Splitting	*29534*	*95.27*
3	3-04	Axial	**Pullout**	***7062***	***22.78***
3	3-05	Axial	Splitting	14342	46.26
3	3-06	Axial	**Bar Fracture**	29646	95.63
3	3-07	Axial	Splitting	15366	49.57
3	3-08	Axial	**Bar Fracture**	29503	95.17
3	3-09	Center	Splitting	25417	81.99
3	3-10	Center	Splitting	25131	81.07

5.1. Influence of Primer

Figure 5-1 shows a typical specimen exhibiting a bond splitting failure. All of the specimens in the scoping study (batch 0) failed through a bond splitting mechanism, as designed. All specimens with primer exhibited larger bar stresses at failure than those without primer. Table 5-2 summarizes the percent change in bar stress due to HMWM primer usage, with positive values indicating larger stress in specimens with primer.

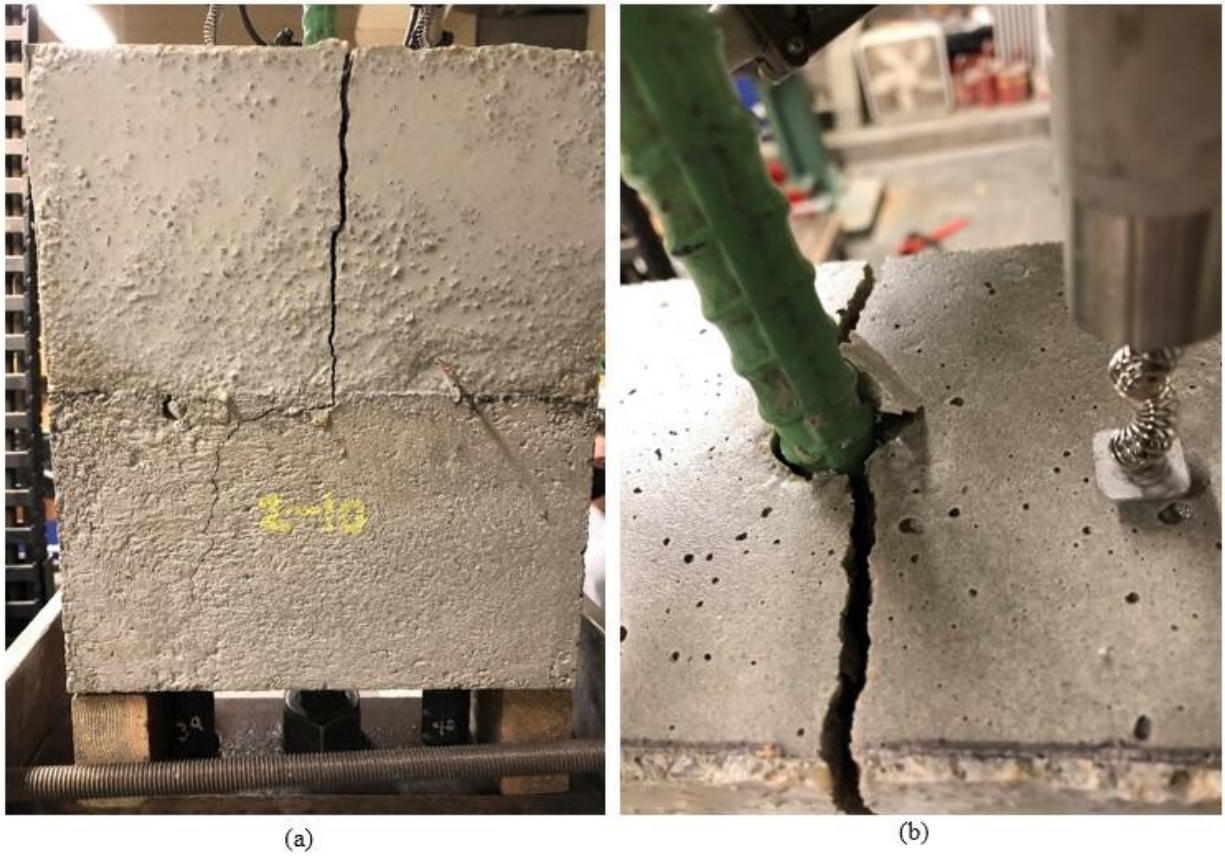

Figure 5-1. (a) Elevation view of splitting failure, 2-10, (b) Splitting at top of HCSC, 2-10

Table 5-2. Percent change in bar stress due to HMWM primer usage

Run	Increase in maximum bar stress with HMWM primer use
0-01p/0-01	10.33%
0-02p/0-02	9.27%
0-03p/0-03	13.99%
0-04p/0-04	1.66%
0-05p/0-05	9.02%
Average	**8.85%**

When using a fractional factorial design (2^{3-1} – Resolution III), confounding occurs with two-factor interactions. However, the main effects are not aliased with one each other and a main effects plot

can be created to assess how each parameter influences the response. Minitab, a statistical analysis software, was used to analyze the results of the non-contact splice tests (Minitab 2022) and create regression equations for bar stress as a function of the input parameters (splice length, side cover, and temperature).

Figure 5-2 shows the main effects of the specimens with and without the use of HMWM primer. The blue line shows the bar stress response for the range of the factorial points. The red dot is the measured center point data. For specimens with and without HMWM primer, bar stress increased as splice length and side cover were increased, as expected. The decrease in bar stress with increases in testing temperature is consistent with the relationship between HCSC strength and temperature from the mechanical characterization testing. The same trends are found in the main effects plot for the specimens with HMWM primer.

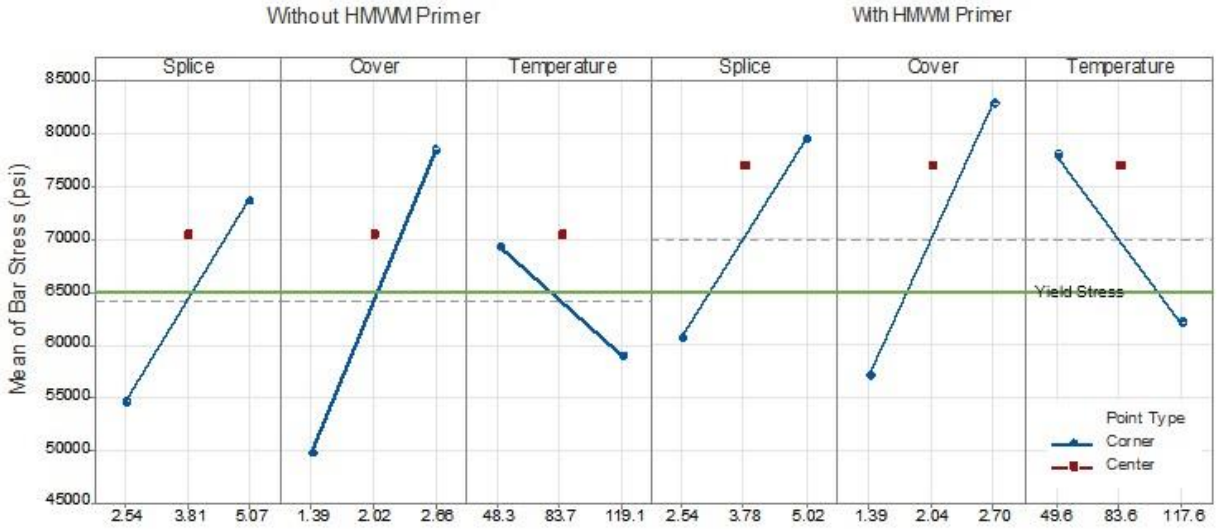

Figure 5-2. Main effects of usage of HMWM primer

The bar stress for the tests with and without HMWM primer is above bar yield for the center point of the design space. There is a vertical shift between the two main effects plots indicating that the usage of primer does affect the observed bar stress. The overall mean of bar stress for specimens without HMWM primer was 64.1 ksi while specimens with HMWM primer had an average of 69.9 ksi, a 9% increase in bar stress. The use of HMWM primer is, therefore, recommended based on the testing results and by the manufacturer. The usage of primer would allow for smaller joint widths due to reducing splice length and cover requirements to reach bar yielding.

5.2. Influence of Temperature, Splice Length, and Bar Cover

Figure 5-1, Figure 5-3, and Figure 5-4 show the failure patterns that were observed in the test program. The majority of specimens failed through a bond splitting mechanism (Figure 5-1), as designed. The remainder failed through fracturing of the embedded reinforcement (Figure 5-2) or through a pullout mechanism (Figure 5-3). Fracture of the reinforcement was observed at the extremities of the experimental design space, as expected: at lower test temperatures, longer splice lengths, larger side covers, and smaller bar diameters, when compared to the center of the design space.

(a) (b) (c)

Figure 5-3. (a) Elevation view of bar fracture, 1-02, (b) Rebar at top of HCSC, 1-02, (c) Bar fracture and top of HCSC, 1-04

(a) (b)

Figure 5-4. (a) Elevation view of pullout failure, 2-04, (b) Pullout at top of HCSC, 2-04

5.3. Batch-to-Batch Variability

Table 5-3 compares the measured bar stress at failure for the six nominally identical center point specimens (for reference the yield and ultimate strength of the reinforcement were 65.0 ksi and 96.0 ksi, respectively). Because the experimental design was conducted using three separate batches of HCSC, an important consideration was the batch-to-batch variability of the repeated center point. In each batch, two specimens were tested with identical properties, the center point of the design space (T =75 °F, ℓ_s = 3.75 in, c_b = 2.0 in, and d_b = 0.625 in). This comparison also considers the inherent variability between specimens due to small construction, conditioning, and testing differences. The strength of the CCD design is the ability to quantify and incorporate this variability in analyzing the experimental results. The very low coefficient of variation between the six specimens (<5%) shows that the batch-to-batch variation was minimal.

Table 5-3. Bar stress at failure for repeated center point specimens

Run	Bar Stress (ksi)
1-09	85.7
1-10	82.7
2-09	79.0
2-10	81.4
3-09	82.0
3-10	81.1
Mean	82.0
Standard Deviation	2.2
Coeff. Of Variation	2.7 %

5.4. Stress-Slip Behavior

For each parameter, two specimens were tested with either an extreme high or low value of the experimental variable. All other parameters were kept the same as the center point. These "star" points are compared to the center point specimens in Figure 5-5, Figure 5-6, Figure 5-7 and Figure 5-8. The equivalent stress-front-end displacement curve of a No. 5 epoxy-coated rebar is also plotted for reference, which was computed by multiplying the strain values from the measured stress-strain response of a bare bar by the free length, 4 in between the HCSC surface and the point where the LVDTs were attached to the epoxy-coated reinforcement in the test specimens. The difference between the specimen behavior and the dashed reference line can, therefore, be interpreted as the contribution of bond slip to the overall specimen response.

The temperature star points (5 °F and 145 °F) show the range in behavior of HCSC at high and low temperatures (Figure 5-5). For the specimen tested at a low temperature, a small yield plateau and high bar stress at failure was observed. The stress-strain curve is stiffer than the center point and has high bond strength, shown by the small difference between the curve of the reinforcement and the specimen. It is important to note that the behavior is of the composite specimen, not HCSC individually. Though the observed failure method observed was bond splitting, the bar stress was 95.3 ksi, very close to the tensile strength of the bar. The specimen tested at a high temperature did not reach bar yield and is much less stiff than the center point, failing by bar pullout.

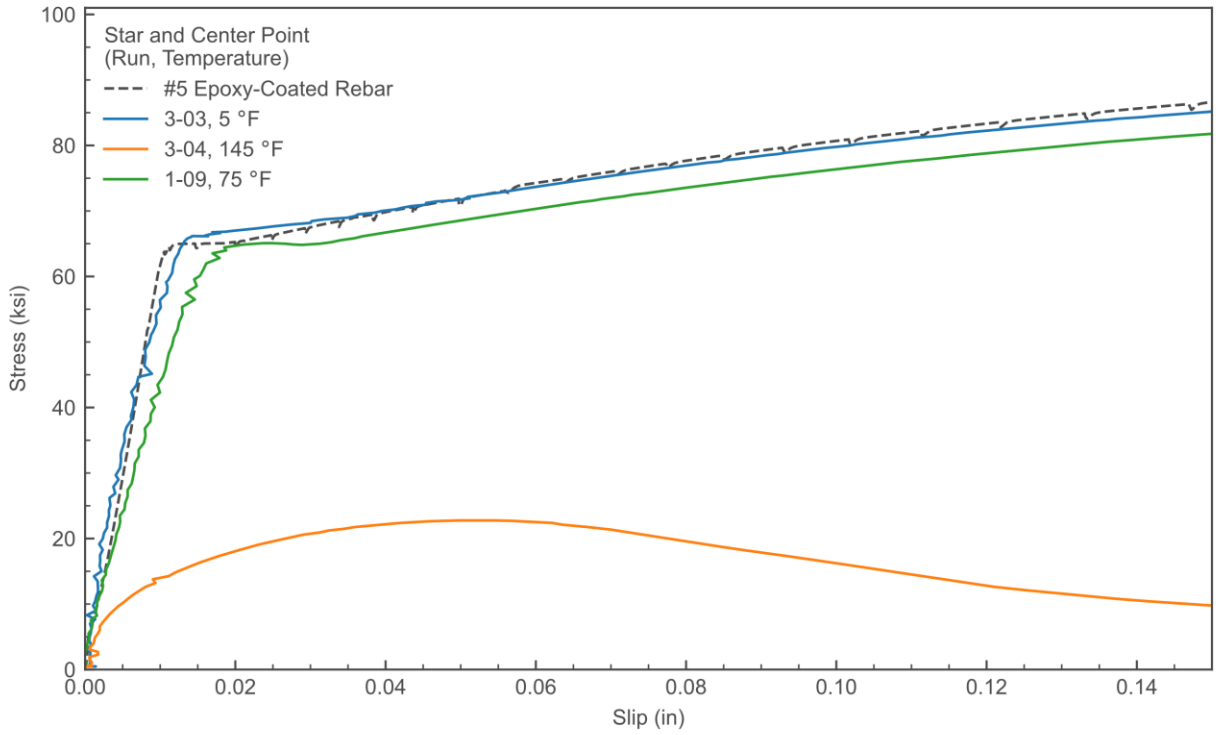

Figure 5-5. Stress-front end displacement for temperature star points and center points

Figure 5-6 and Figure 5-7 show the star points for splice length (1.25 in. and 6.25 in.) and side cover (0.75 in. and 3.25 in.), respectively. The extreme low parameters for both splice length and side cover exhibit similar behavior. Both specimens with minimal splice length or side cover failed via splitting with bar stresses below yield. The stiffness of the specimens was similar to the center points, until close to failure. The stress-strain behavior is quite brittle, due to the poor confinement and lack of bond development. The specimens with large splice length or side cover both failed due to bar fracture. Sufficient bond could be developed such that the specimens could withstand loading larger than the tensile strength of the reinforcement. The stress-strain curves have similar stiffnesses and yield plateaus compared to the center point.

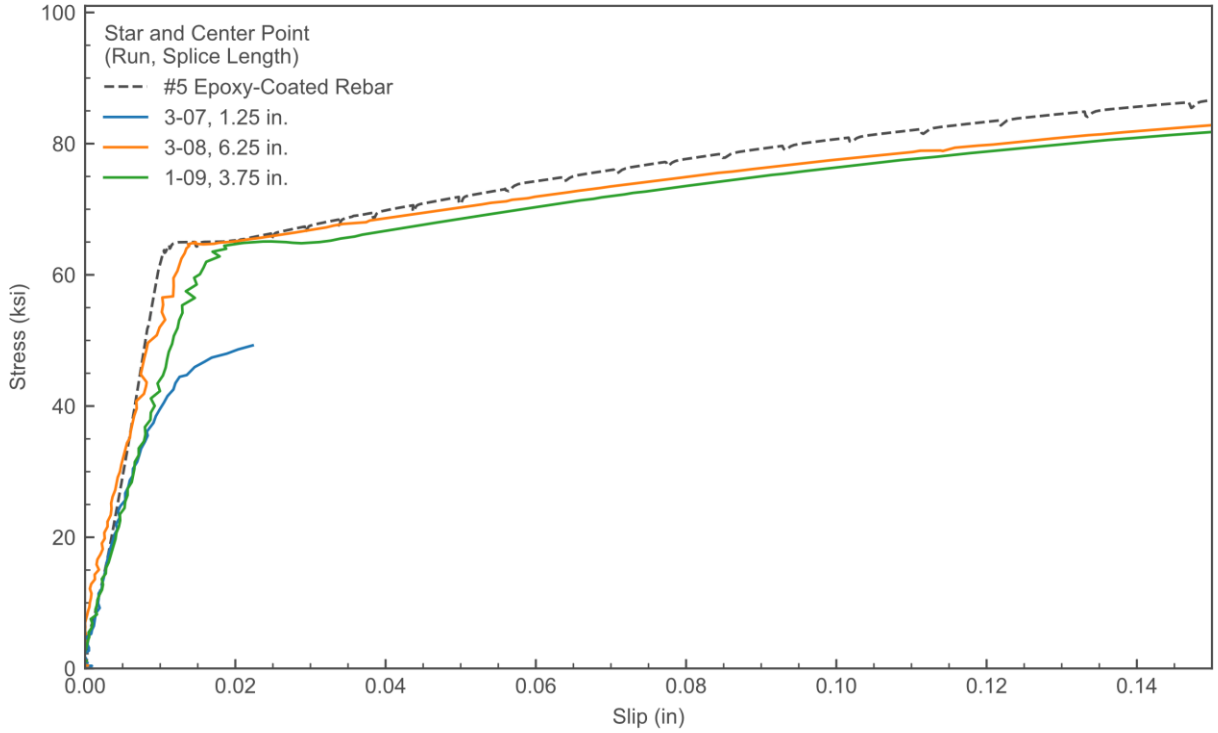

Figure 5-6. Stress-front end displacement for splice length star points and center points

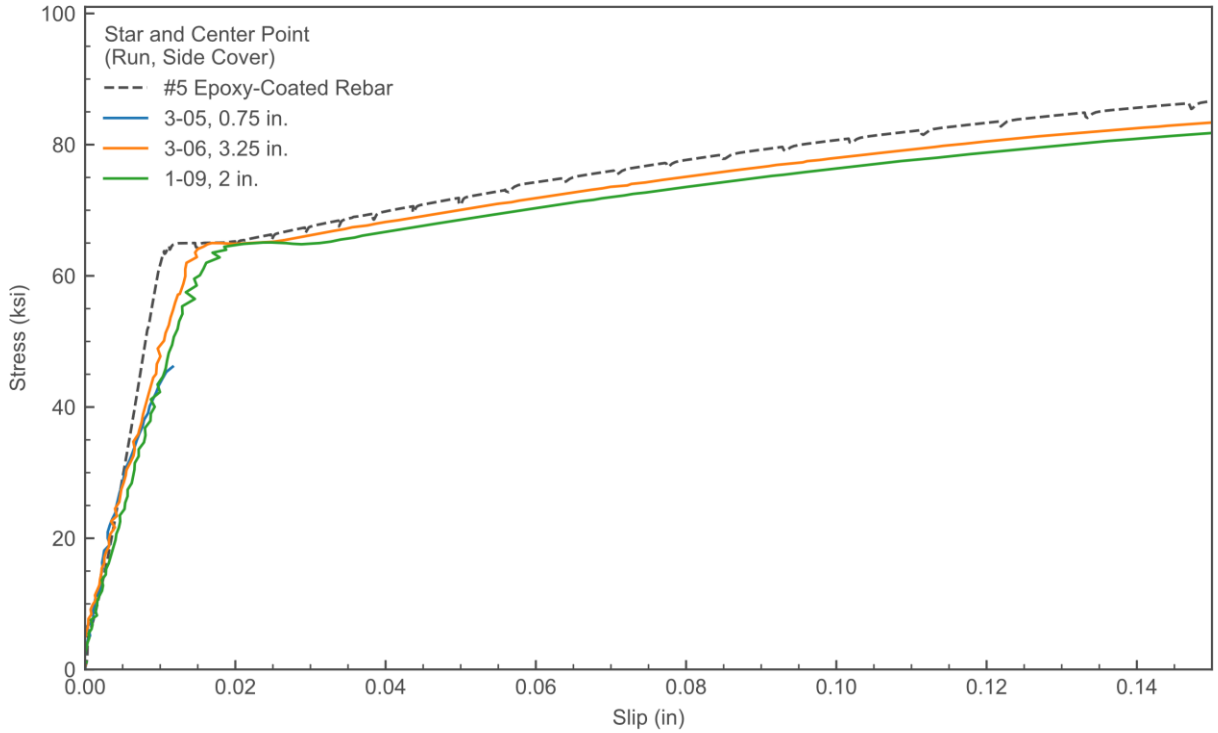

Figure 5-7. Stress-front end displacement for side cover star points and center points

Figure 5-8 shows the response of the specimens with the extreme values of bar diameter (0.375 in. and 0.875 in.). Bar diameter affected the load that could be applied to the specimen before bar failure and also changed the normalized splice length and side cover (relative to the bar diameter). The specimen with a No. 3 bar (0.375 in diameter) failed due to bar fracture, while the specimen with a No. 7 bar (0.875 in diameter) failed due to a bond splitting of the specimen. Prior to reaching the yield stress of the reinforcement.

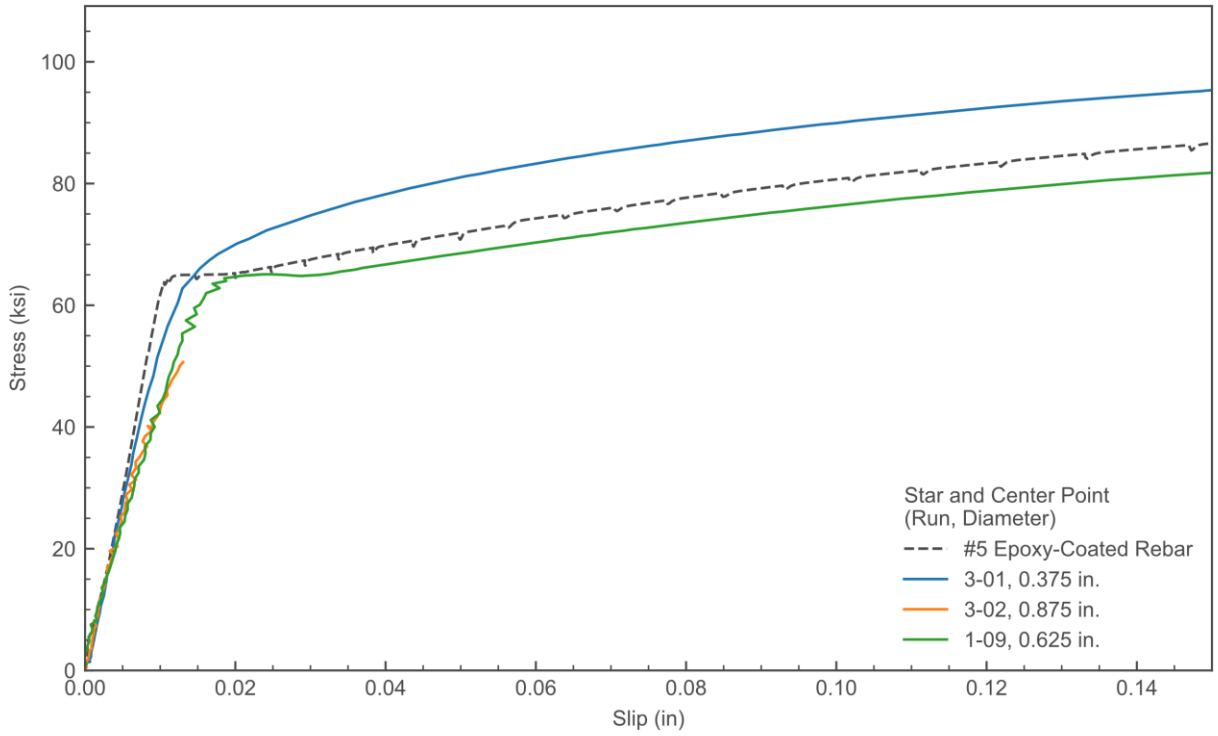

Figure 5-8. Stress- front end displacement for bar size star points and center points

5.5. Maximum Bar Stress

Figure 5-9 compares the normalized splice length in terms of the number of bar diameters and bar stress for the main specimens in the non-contact splice tests. Temperature is shown based on the color of the marker. Only specimens with greater than three bar diameters of cover are shown. Also shown is data from non-contact splice tests using non-proprietary UHPC, from Peruchini et al. (2017), with similar splice lengths, bar diameters, and side cover. For increasing splice lengths, the bar stress increases, eventually resulting in bar fracture once stresses in the specimen exceed the ultimate strength of the reinforcement. Specimens tested at colder temperatures failed at higher bar stressed for the same splice length. The bar stresses of the reinforcement embedded in HCSC are comparable to those in UHPC, indicating similar bond performance, especially at room temperature or colder temperatures. Specimens with splice lengths larger than five bar diameters consistently failed above bar yield, even at elevated temperatures.

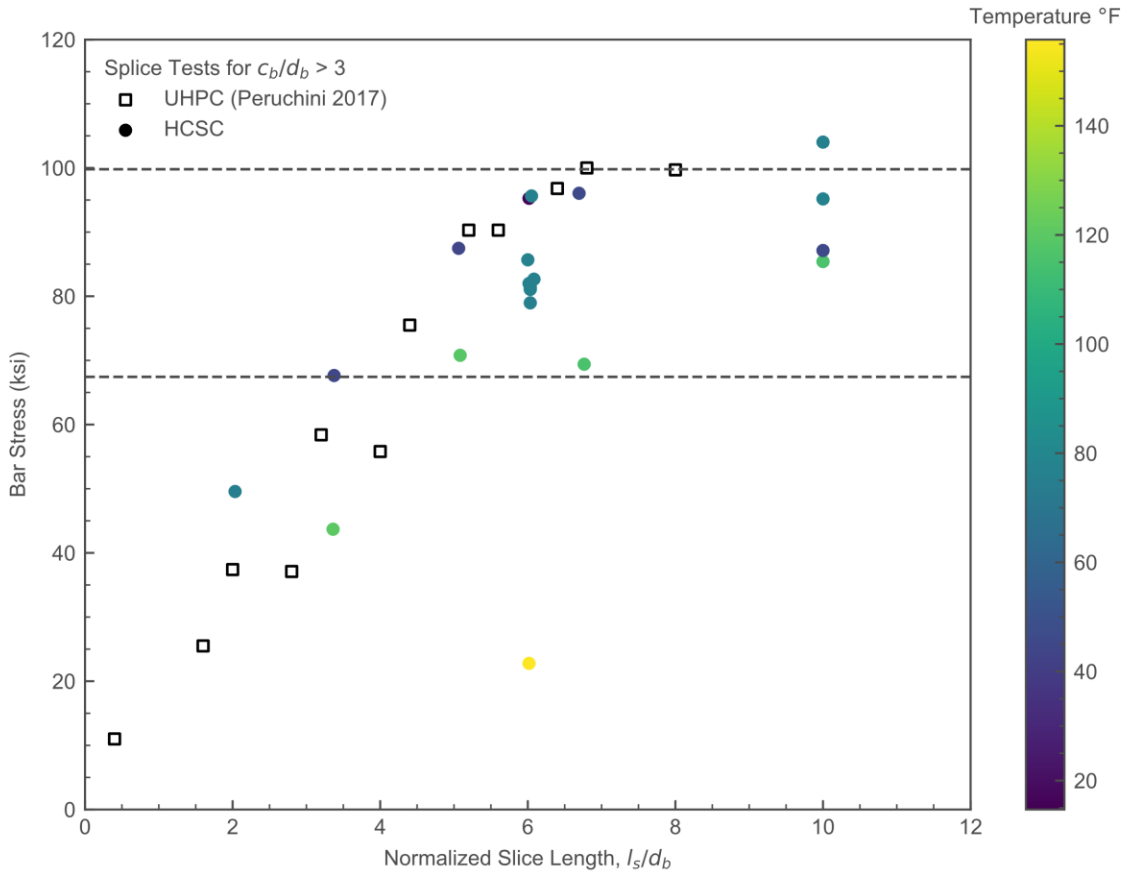

Figure 5-9. Comparison of normalized splice length and peak bar stress

Using the measured geometry of each specimen and the measured surface temperature at the start of testing, a regression analysis was performed in Minitab for the non-contact splice specimens. Analysis of variance testing (ANOVA) and response surface methodology (RSM) were used to create a model to explore the relationship between maximum bar stress and the geometric testing parameters.

The four-factor CCD design allows for linear, square, and two-way interaction terms. Table 5-4 shows the initial model with all combinations of terms and the terms that were included in the final model, which was reduced to only include significant terms. The final equal to model bar stress is shown at the bottom of the table. F-values and P-values were used to determine each term's significance. Terms with large P-values were removed from the model as the null hypothesis of a term being statistically insignificant can be rejected. Though P-values are typically kept below a significance level of 0.05, some terms were kept in the selected model terms to prevent entire term types (linear, square, or two-way interaction) from being excluded from the model. Additionally, terms were retained to capture the physical phenomena that were observed in both material characterization and during non-contact splice testing.

Table 5-4. Analysis of Variance Results

Sources	All Terms F-Value	All Terms P-Value	Selected Terms F-Value	Selected Terms P-Value
Model	10.99	0.00004	18.70	0.00000
Blocks	0.33	0.72300	0.38	0.68931
Linear	37.49	0.00000	45.77	0.00000
Temperature (T)	44.34	0.00002	52.19	0.00000
Bar Diameter (d_b)	48.89	0.00001	58.36	0.00000
Splice Length (ℓ_s)	28.91	0.00013	35.12	0.00001
Side Cover (c_b)	30.67	0.00010	40.06	0.00001
Square	4.23	0.02067	6.32	0.00407
Temperature × Temperature	13.76	0.00262	15.59	0.00094
Diameter × Diameter	0.98	0.34074	-	-
Splice Length × Splice Length	3.08	0.10272	3.13	0.09367
Side Cover × Side Cover	3.65	0.07826	3.65	0.07224
2-Way Interaction	1.30	0.32281	3.88	0.03970
Temperature × Diameter	0.45	0.51341	-	-
Temperature × Splice Length	0.12	0.73138	-	-
Temperature × Side Cover	0.59	0.45444	-	-
Diameter × Splice Length	1.77	0.20570	2.06	0.16847
Diameter × Side Cover	4.80	0.04729	5.77	0.02726
Splice Length × Side Cover	0.00	0.97652	-	-

$$BarSress = 136113 + 466\mathrm{T} - 287725 d_b + 8899 \ell_s + 7841 c_b - 4.59 T^2 - 1663\, {\ell_s}^2 - 7148 {c_b}^2 + 17759 * d_b * \ell_s + 60473 * d_b * c_b$$

The model was then used to create the main effects plot, Figure 5-10, and the interaction plot, Figure 5-11, for each parameter and its associated interactions. The main effect plot created for the CCD analysis is based on the bar stress model as opposed to the individual data points. The trends in the CCD main effects plot are similar to the results from the scoping study, however, there is curvature in the trend lines due to higher order terms being included in the bar stress model.

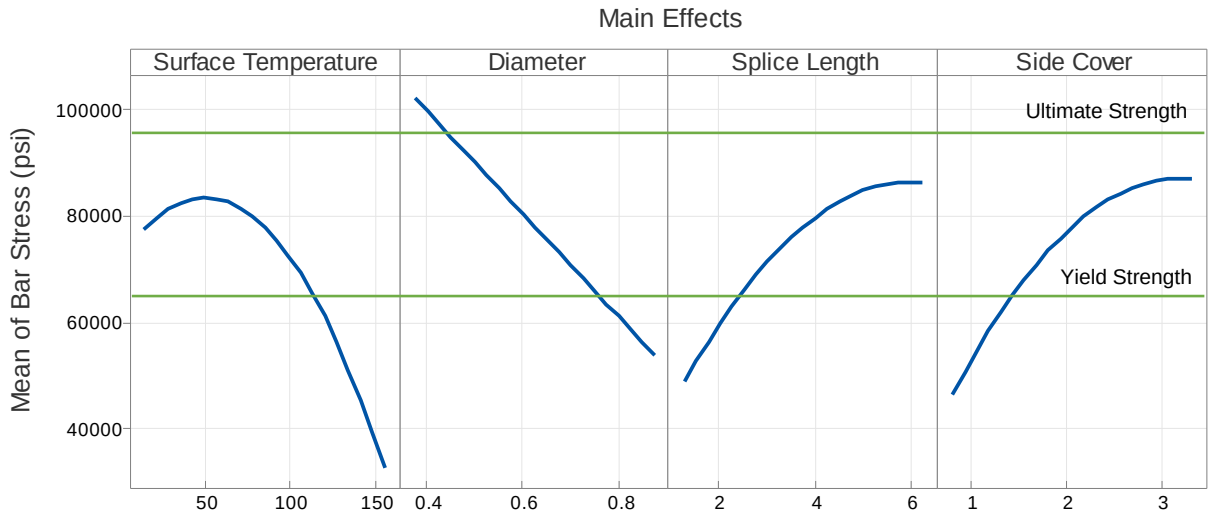

Figure 5-10. Main effects of CCD analysis

Similar to the mechanical characterization and the scoping study, larger bar stresses and material strengths were measured for specimens conditioned to lower temperatures. At elevated temperatures, the reverse was true, the material strength and bar stresses were reduced. As expected, increases in splice length and side cover resulted in larger bar stresses at specimen failure. The parabolic shape for the surface temperature, splice length, and side cover curves captures the physical limit of bar fracture on bar stress. For temperatures below 50 °F, the reduction in bar stress is non-physical, i.e., it occurs because the model is not able to form a flat plateau. The square term of diameter was removed from the model, resulting in a linear influence of bar diameter on bar stress.

Figure 5-11 displays the two-way interaction terms and their effects on bar stress at failure. Each panel is broken up into the low, mean, and high parameter levels for one of the interactions. Interactions between splice length and side cover are not shown as the two-way interaction term were not included in the model due to a lack of statistical significance. Additionally, temperature has no significant terms for two-way reactions, so it is also not included as a panel in the interaction diagram. The interaction between splice length and bar diameter and side cover and bar diameter were similar. Both interactions support the idea that side cover and splice length could be normalized by the bar diameter. Once normalized, the three curves in the top panes would shift horizontally from one another, forming an increasing, asymptotic relationship as one would expect (similar to the main effects plots in Figure 5-10).

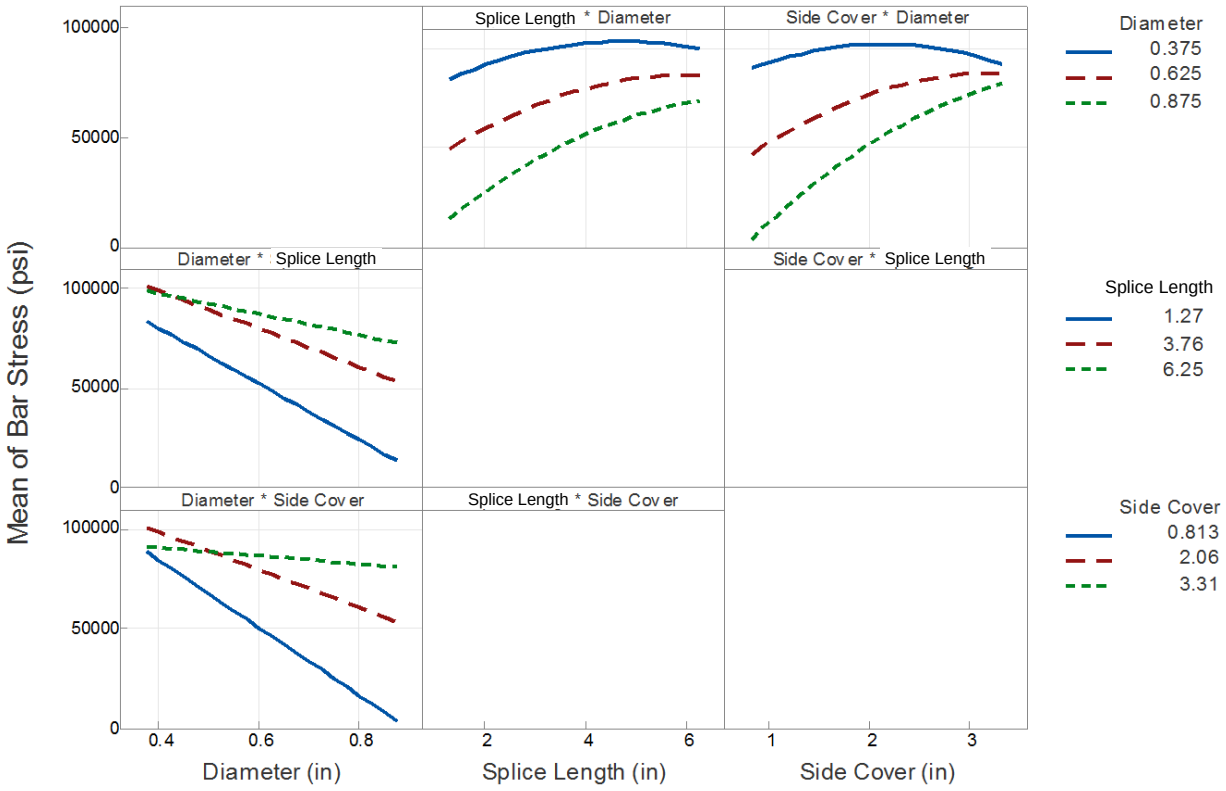

Figure 5-11. Interaction diagram of CCD analysis

CHAPTER 6. DESIGN RECOMMENDATIONS

In ABC, precast elements are often used to expedite project delivery, improve project quality, and reduce traffic disruptions. Once delivered on-site, adjacent precast superstructure elements are connected at closure joints. To complete the superstructure, the closure joints are filled with a field-cast material that creates continuity between the precast concrete elements by splicing the reinforcement protruding from the adjacent precast members within the joints. The geometry of the closure joints, the speed at which the connections can be completed, the curing time before the bridge can be opened to traffic, and the cost of the system are all dependent on the material that is used to fill the gaps between precast elements. Closure joint geometry is largely determined by the strength of closure pour material, particularly bond strength. Potential alternatives considered here include conventional cementitious concrete, UHPC, and HCSC.

Figure 6-1 shows an example joint geometry and reinforcement for a conventional cementitious concrete closure pour (from Garber and Shahrokhinasab 2019). This detail could be used for both transverse longitudinal joints. A minimum joint width of 12 in is specified by AASHTO. This width allows for adequate development of bonding between the concrete and reinforcement. The AASHTO LRFD Bridge Construction Specifications require vertical joints to be keyed. The preparation of the joint is important to ensure an adequate bond, typically an exposed aggregate finish. Additionally, the concrete in the closure joint should have the strength comparable to the precast components (Section 5.14). Per Section 5.11, the AASHTO specified basic development, $\ell_{d,}$ for No. 11 bars and smaller is $1.25A_b f_y/\sqrt{f'_c}$ and no less than 0.4 $d_b f_y$. The minimum splice length for reinforcement in tension is 12 in and no less than $\ell_{d.}$

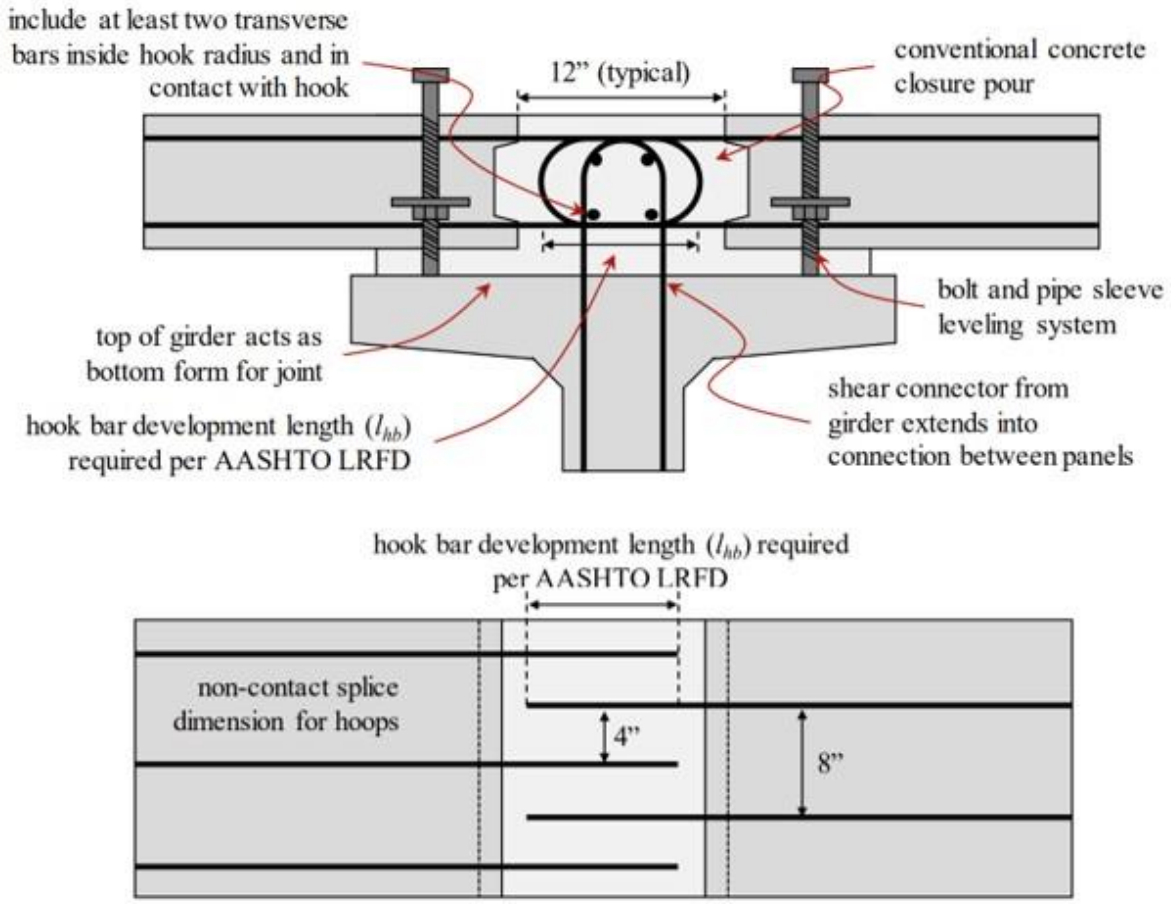

Figure 6-1. Conventional concrete closure joint per AASHTO specifications (Garber and Shahrokhinasab 2019)

Figure 6-2 shows an example of a UHPC closure joint detail. Research conducted by the FHWA (Graybeal 2014) provides guidance on the structural design of closure joints that have been adopted into the AASHTO LRFD Guide Specifications for Accelerated Bridge Construction (AASHTO 2018). This guidance recommends the minimum embedment length of deformed steel reinforcement, ℓ_d, be taken as 8 d_b for No. 8 bars or smaller with f_y less than or equal to 75 ksi. The embedment length recommendation requires that the cover be greater than or equal to 3db with UHPC having a compressive strength of at least 14 ksi and 2% fibers by volume. The splice length for straight deformed steel reinforcement is recommended to be at least 0.75 ℓ_d, or 6 d_b if a development length ℓ_d = 8 d_b is used. This results in a minimum joint width of 10 d_b with some allowance for construction tolerance in the field.

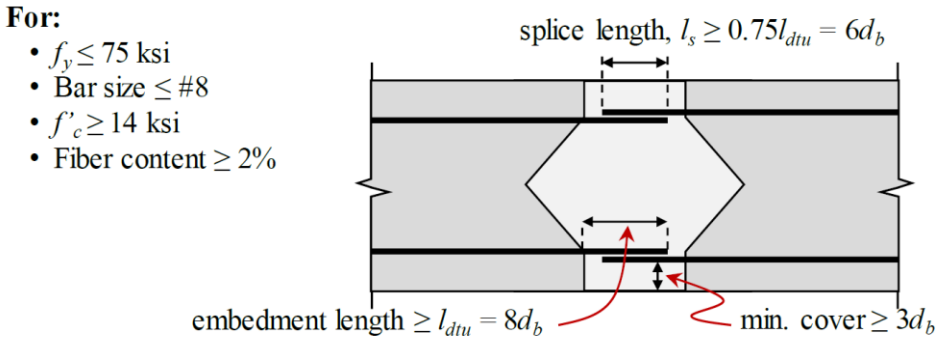

Figure 6-2. UHPC Recommended joint geometry (Garber and Shahrokhinasab 2019)

If HCSC in combination with HMWM primer is used, sufficient bond strength would be developed with the minimum AASHTO specified joint width, splice length, and development length. This however is impractical since HCSC is considerably stronger than conventional concrete and can thus be utilized in a more efficient joint geometry. Instead, the material strengths should be used to determine the required joint width based on the bond strength the closure joint material provides. The parameters that influence bond strength are the material properties, splice length, side cover, bar size, and temperature. The materials assumed to be used in this discussion are HCSC and epoxy-coated reinforcement, identical to the tested specimens. Since multiple parameters were changed for each specimen during testing, selecting a particular specimen geometry to be used would not necessarily isolate the most efficient combination of parameters. Instead, the statistical regression model combining test temperature, bar size, splice length, and side cover can be used to determine suitable regions of the design space.

Figure 6-3 shows the mean surface created from the statistical regression of the data. The panes from top to bottom show the variation in temperature, the panes from left to right show the variation in bar size. Each pane shows the achieved bar stress as a function of both the normalized splice length and normalized side cover. The black dashed line denotes the yield strength, and the grey line denotes the ultimate strength of the reinforcement. The white dashed lines shows the UHPC closure joint design recommendation by the FHWA (Graybeal 2014). The design area for UHPC is, therefore, the upper right corner, in which sufficient cover and splice length is provided.

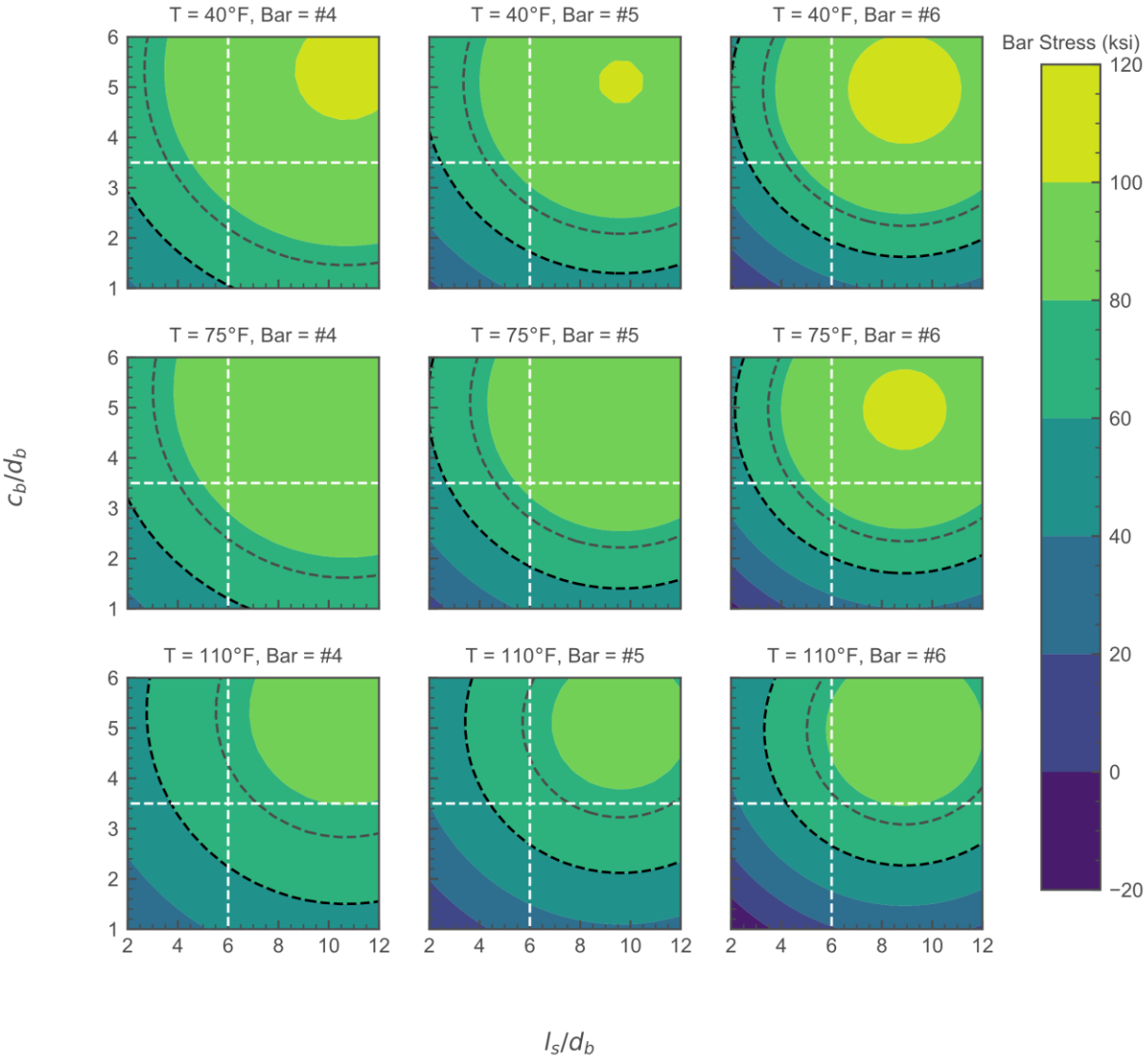

Figure 6-3. Bar stress for varying temperatures and bar sizes

Based on the results of the mechanical properties tested, the material and therefore bond strength of HCSC varies with temperature. However, when used in a closure joint the relative volume of HCSC with respect to cementitious concrete is small. The large volume and thermal mass of concrete would help stabilize and reduce the temperature range of the PC. A conservative temperature was selected for the design recommendation, though additional adjustments should be made based on the known service temperatures of the project location. For the bar sizes and temperatures shown, the design space specified by the FHWA is sufficient for bar yield at the most conservative edge (110 °F and No. 6 bars).

Based on a statistical analysis of the collected non-contact splice data, epoxy-coated deformed bar reinforcement embedded in HCSC with at least a 6db splice length and 3db clear cover is sufficient for developing the full yield stress of the reinforcement for temperatures less than or equal to 110 °F, on average. Above this temperature, additional splice length or bar cover would be required to

ensure bar yield before material failure. These results support the use of similar joint geometries for both HCSC and FRPC. The capability of FRPC to have the same joint geometry as UHPC helps increase the potential options for a given ABC project.

It should be noted that both the recommendations for HCSC and UHPC closure joint geometries (see Graybeal et al. YYYY) are unfactored and are based on the splice length required to achieve 75 ksi in the epoxy-coated reinforcement at minimum. Additionally, research by Peruchini et al. 2017 concluded that simulated deck specimens exhibited a 14% lower strength than that implied by the non-contact lap-splice tests using the same UHPC material with the same cover and embedment length. The difference in bond strength from non-contact splice testing to a more realistic bridge deck geometry should be further explored and incorporated into the joint width and reinforcement design.

The use of primers aid in the adhesion of HCSC and other PCs to the adjoining elements and reinforcement. From the scoping study completed, the use of an HMWM primer increases bond by an average of 9%. Joint designs should include the use of primer, whenever feasible. Proper preparation and application of primer should be used to ensure proper bond behavior.

The preparation of the bond line surface and reinforcement is critical to ensure good bond between the closure joint material and the precast element. HCSC and other PCs have excellent bond to itself, reinforcement, and conventional cementitious concrete at connection interfaces with sufficient surface preparation. Good bonding has been shown at interfaces with an exposed aggregate finish. The exposed aggregate finish can be created by applying a retarder to the formwork when casting the precast segments. After form removal, the unhydrated paste can be washed, brushed, or blast off, exposing a rough aggregate surface. Alternatively, abrasive blasting can be used to remove contaminants, open pore structure, and expose aggregate. It is recommended that for closure joints a roughed surface with current best practices be used to provide an exposed aggregate finish.

For closure joints between precast girders, the splice length should account for any sweep that may occur in the structure. The minimal splice length over the length of the closure joint should be ensured in designs and that adequate edge cover is maintained. For closure joints in precast deck panels or precast girders without additional deck overlay, minimum side cover requirements should account for any cross slope or camber of the elements. These two practical considerations may lead to more conservative nominal joint geometries than the minimum dimensions presented.

CHAPTER 7. SUMMARY, CONCLUSIONS, AND FUTURE WORK

The use of FRPC as a closure joint material in ABC applications was evaluated as a potential alternative to conventional cementitious concrete and UHPC.

The mechanical properties of HCSC were investigated to determine the effects of temperature and strength gain over time. Three different properties were studied: compressive strength, modulus of rupture, and bond pullout strength. Six batches were mixed, cast, and tested – two batches per property, one for temperature effects and one for early strength gain. For temperature effects, specimens were cast and cured at ambient temperatures and then conditioned to four different testing temperatures, spanning the range of service temperatures in western Washington. To capture the effects of early strength gain, specimens were mixed and cast then tested at early and frequent intervals, starting at two hours after mixing through seven days.

Based on the results of the mechanical characterization, splice length, side cover, bar size, and temperature were chosen as parameters for further investigation, and their ranges were selected for non-contact splice testing. First, a single batch of non-contact splice specimens was tested to determine the effect of the HMWM primer on the bar stress at failure. After demonstrating the benefits that the HMWM primer had on bond strength, three blocks of ten specimens apiece were cast with parameters (test temperature, T; splice length, ℓ_s; side cover, c_b; and bar diameter, d_b) ranging based on the central composite rotatable experimental design.

Using the collected data, the relationship between the maximum bar stress and splice length, side cover, bar size, and test temperature was estimated by fitting a regression surface. This allowed the isolation of the individual effects of each parameter. Using these insights, a closure joint width and reinforcement development recommendations were made for the use of HCSC as a closure joint material.

The following conclusions were drawn from the study:

- FRPC exhibits significant variation in mechanical properties with temperature. For HCSC, a temperature increase of 40 °F resulted in a roughly 25% reduction in material strength, which was consistent between the compression, flexure, and bond tests. The opposite was true for decreases in temperature.
- There is a tradeoff between working time and the rate of strength development for HCSC. If shorter working times can be tolerated, significant strength (70% of the 7-day value) can be achieved within 2 hours after mixing.
- The development of early compressive, flexure, and bond strengths were very similar. For the level of accelerator used in this study (3% by volume initiator), the compressive, flexural, and bond strengths were roughly 70%, 80%, and 75% of their 7-day values, respectively, 4 hours after mixing.
- For non-contact lap splices embedded in HCSC, the use of HMWM primer increased the bar stress at failure by roughly 9%. The same general trends on the influence of temperature, splice length, and side cover were similar between specimens with and without HMWM primer.
- In non-contact splice specimens, increases in splice length and side cover result in increases in bar stresses at failure. The testing temperature has the opposite effect, with bar stress decreasing as temperature increases.
- Based on RSM analysis of the results of the non-contact splice testing, the AASHTO

recommendations for closure joint geometry for UHPC are also applicable for HCSC up to temperatures of 110 °F. Above 110 °F, additional splice length or bar cover would be required to ensure bar yield before material failure.

Following the promising results of this exploratory study, future testing is proposed to address additional design considerations, which were beyond the scope of the present project. Full-scale strength and fatigue testing using sample joint configurations should be completed to validate the behavior of FRPC bond in field scale geometries at different temperatures.

Additionally, there is a dearth of research to understand the long-term creep characteristics of PCs, although it is well understood that most polymers exhibit significant creep deformations under sustained loads (Hsu 1984). The knowledge of the creep behavior of PCs, like HCSC, is important to understand how the long-term loading affects the overall structure. Creep deformations at joints between precast elements may lead to redistribution of forces to adjacent elements, which may not have been accounted for in design. There are also potential opportunities to leverage the unique time-dependent properties of PC to solve current issues in bridge design. For both of these reasons, the creep characteristics of PCs should be further studied.

REFERENCES

Abdel-Fattah, H., and M. M. El-Hawary. 1999. "Flexural behavior of polymer concrete." Construction and Building Materials, 13 (5): 253–262. https://doi.org/10.1016/S0950-0618(99)00030-6.

Abokifa, M., and M. A. Moustafa. 2021. "Experimental behavior of poly methyl methacrylate polymer concrete for bridge deck bulb tee girders longitudinal field joints." Construction and Building Materials, 270: 121840. https://doi.org/10.1016/j.conbuildmat.2020.121840.

Aboutaha, R. S., E. M. Lui, G. Martin, P. Petrina, L. Phoenix, and E. Giannelis. 2005. "Investigation of Durability of Wearing Surfaces for FRP Bridge Decks." 397.

ACI. 2019. Polymer Concrete: Guidelines for Structural Applications (ACI 548.6R-19). Farmington Hills, MI, USA: Committee 548, American Concrete Institute.

Al-Negheimish, A. I. 1988. "Bond strength, long term performance and temperature induced stresses in polymer concrete-portland cement concrete composite members."

American Association of State and Highway Transportation Officials. 2012. AASHTO LRFD Bridge Design Specifications. Washington, DC: AASHTO.

American Association of State Highway and Transportation Officials. 2018. AASHTO LRFD guide specifications for accelerated bridge construction. Washington, DC. AASHTO

Anderson, K., M. Russell, K. Littleton, D. McKernan, J. Uhlmeyer, J. Weston, and C. Simonson. 2013. Polyester Polymer Concrete Overlay. Tumwater, WA: Washington State Department of Transportation.

ASTM. 2019. A775/A775M - Standard Specification for Epoxy-Coated Steel Reinforcing Bars. West Conshohocken, PA: ASTM International.

ASTM. 2020a. D7913/D7913M - Standard Test Method for Bond Strength of Fiber-Reinforced Polymer Matrix Composite Bars to Concrete by Pullout Testing. West Conshohocken, PA: ASTM International.

ASTM. 2020b. A370 - Standard Test Methods and Definitions for Mechanical Testing of Steel Products. West Conshohocken, PA: ASTM International.

ASTM. 2021a. C39/C39M - Standard Test Method for Compressive Strength of Cylindrical Concrete Specimens. West Conshohocken, PA: ASTM International.

ASTM. 2021b. C78/C78M - Standard Test Method for Flexural Strength of Concrete (Using Simple Beam with Third-Point Loading). West Conshohocken, PA: ASTM International.

ASTM. 2022. A706/A706M Specification for Deformed and Plain Low-Alloy Steel Bars for Concrete Reinforcement. West Conshohocken, PA: ASTM International.

Box, G. E. P., J. S. Hunter, and W. G. Hunter. 2005. Statistics for experimenters: design, innovation, and discovery. Wiley series in probability and statistics. Hoboken, N.J: Wiley-Interscience.

Carreira, D. J., and K.-H. Chu. 1985. "Stress-Strain Relationship for Plain Concrete in Compression." JP, 82 (6). https://doi.org/10.14359/10390.

Fowler, D. W. 1999. "Polymers in concrete: a vision for the 21st century q." 4.

Fowler, D. W., A. H. Meyer, and D. R. Paul. 1981. “Techniques to Improve Strength of Polymer Concrete Made with Wet Aggregate.” 16.

Fowler, D. W., and D. W. Whitney. 2012. Long-Term Performance of Polymer Concrete for Bridge Decks. 14623. Washington, D.C.: National Cooperative Highway Research Program.

Garber, D., and E. Shahrokhinasab. 2019. “ABC-UTC Guide for: Full-Depth Precast Concrete (FDPC) Deck Panels.”

Graybeal, B. 2014. Bond Behavior of Reinforcing Steel in Ultra-High Performance Concrete. Washington, D.C.: USDOT FHWA.

Graybeal, B. A. 2006. Material Property Characterization of Ultra-High Performance Concrete. 188. Washington, D.C.: USDOT FHWA.

Guedes, R. M., C. M. L. Tavares, and A. J. M. Ferreira. 2004. “Experimental and theoretical study of the creep behavior of GFRP-reinforced polymer concrete.” Composites Science and Technology, 64 (9): 1251–1259. https://doi.org/10.1016/j.compscitech.2003.10.004.

Haber, Z. B., and B. A. Graybeal. 2018. “Lap-Spliced Rebar Connections with UHPC Closures.” J. Bridge Eng., 23 (6): 04018028. https://doi.org/10.1061/(ASCE)BE.1943-5592.0001239.

Haber, Z. B., I. D. la Varga, B. A. Graybeal, Brian Nakashoji, and Rafic El-Helou. 2018. Properties and Behavior of UHPC-Class Materials. Washington, D.C.: USDOT FHWA.

Hassani Niaki, M., A. Fereidoon, and M. Ghorbanzadeh Ahangari. 2018. “Experimental study on the mechanical and thermal properties of basalt fiber and nanoclay reinforced polymer concrete.” Composite Structures, 191: 231–238. https://doi.org/10.1016/j.compstruct.2018.02.063.

Heidari-Rarani, M., M. R. M. Aliha, M. M. Shokrieh, and M. R. Ayatollahi. 2014. “Mechanical durability of an optimized polymer concrete under various thermal cyclic loadings – An experimental study.” Construction and Building Materials, 64: 308–315. https://doi.org/10.1016/j.conbuildmat.2014.04.031.

Hong, S. 2017. “Influence of Curing Conditions on the Strength Properties of Polysulfide Polymer Concrete.” Applied Sciences, 7 (8): 833. https://doi.org/10.3390/app7080833.

Hsu, H.-T. 1984. “Flexural Behavior of Polymer Concrete Beams.” Austin, Texas: The University of Texas of Austin.

Hsu, M., and D. W. Fowler. 1985. “Creep and Fatigue of Polymer Concrete.” ACI Symposium Publication, 89. https://doi.org/10.14359/6256.

Krauss, P. D., and J. S. Lawler. 2018. Bond Behavior of Reinforcing Steel in Kwik Bond Polyester Polymer Concrete. 24. Northbrook, IL: Wiss, Janney, Elstner Associates, Inc.

Kwik Bond Polymers. 2020b. “Product Data Sheet: Hybrid Composite Synthetic Concrete (HCSC).”

Kwik Bond Polymers. 2020a. “Product Data Sheet: PPC 1121 Polyester Polymer Concrete.”

Maas, J. 1997. “I-80—It’s Almost a Decade.” In-Place Performance of Polymer Concrete Overlays, SP-169, 172–179. Farmington Hills, MI: American Concrete Institute.

Maas, J. 2003. “How Polyester Polymer Concrete Highway and Bridge Deck Overlays Became ‘State of the Art.’” Polymers in Concrete: The First Thirty Years, SP-214, 39–49. Farmington Hills, MI: American Concrete Institute.

Mantawy, I., R. Chennareddy, M. Genedy, and M. R. Taha. 2019. “Polymer Concrete for Bridge Deck Closure Joints in Accelerated Bridge Construction.” Infrastructures, 4 (2): 31. https://doi.org/10.3390/infrastructures4020031.

Mebarkia, S., and C. Vipulanandan. 1992. “Compressive Behavior of Glass-Fiber Reinforced Polymer Concrete.” Journal of Materials in Civil Engineering, 4 (1): 91–105. https://doi.org/10.1061/(ASCE)0899-1561(1992)4:1(91).

Minitab. 2022. “Getting Started with Minitab Statistical Software.”

Moustafa, M., A. Itani, and M. Abokifa. 2019. “More Choices for Connecting Prefabricated Bridge Deck Elements.” Reno, NV.

Oussama, E., G. Elhem, V. Mignot, and B. O. Mongi. 2012. “Mechanical and physical properties of epoxy polymer concrete after exposure to temperatures up to 250°C.” Construction and Building Materials, 27 (1): 415–424. https://doi.org/10.1016/j.conbuildmat.2011.07.027.

Park, S.-K., B.-W. Jo, D.-H. Park, and B.-S. Chun. 2010. “Flexural rigidity and ductility of high-strength reinforced polyester polymer concrete beams.” Advances in Cement Research, 22 (2): 91–97. https://doi.org/10.1680/adcr.2010.22.2.91.

Peruchini, T. J. 2017. “Investigation of Ultra-High Performance Concrete for Longitudinal Joints in Deck Bulb Tee.” University of Washington.

Peruchini, T. J., J. Stanton, and P. Calvi. 2017. Investigation of Ultra-High Performance Concrete for Longitudinal Joints in Deck Bulb Tee Bridge Girders. 213. Olympia, WA: Washington State Department of Transportation.

Poillucci, R. A., and C. Hansen. 2013. “Reducing use of styrene monomer in unsaturated polyester resins.” 23.

Qiao, P., Z. Zhidong, and S. Allena. 2016. Developing Connections for Longitudinal Joints between Deck Bulb Tees -- Development of UHPC Mixes with Local Materials. 119. Olympia, WA: Washington State Department of Transportation.

Reis, J. 2005. “Mechanical characterization of fiber reinforced Polymer Concrete.” Mat. Res., 8 (3): 357–360. https://doi.org/10.1590/S1516-14392005000300023.

Reis, J. M. L., and A. J. M. Ferreira. 2006. “Freeze–thaw and thermal degradation influence on the fracture properties of carbon and glass fiber reinforced polymer concrete.” Construction and Building Materials, 20 (10): 888–892. https://doi.org/10.1016/j.conbuildmat.2005.06.021.

Ribeiro, M. C. S., P. R. Nóvoa, A. J. M. Ferreira, and A. T. Marques. 2004. “Flexural performance of polyester and epoxy polymer mortars under severe thermal conditions.” Cement and Concrete Composites, 26 (7): 803–809. https://doi.org/10.1016/S0958-9465(03)00162-8.

Ribeiro, M. C. S., J. M. L. Reis, A. J. M. Ferreira, and A. T. Marques. 2003a. "Thermal expansion of epoxy and polyester polymer mortars—plain mortars and fibre-reinforced mortars." Polymer Testing, 22 (8): 849–857. https://doi.org/10.1016/S0142-9418(03)00021-7.

Ribeiro, M. C. S., C. M. L. Tavares, M. Figueiredo, A. J. M. Ferreira, and A. A. Fernandes. 2003b. "Bending characteristics of resin concretes." Mat. Res., 6 (2): 247–254. https://doi.org/10.1590/S1516-14392003000200021.

Sett, K., and C. Vipulanandan. 2004. "Properties of Polyester Polymer Concrete with Glass and Carbon Fibers." ACI Materials Journal, 101 (1). https://doi.org/10.14359/12985.

Shahrokhinasab, E., and D. Garber. 2021. Development of "ABC-UTC Non-Proprietary UHPC" Mix. FIU.

Sika. 2020. "Product Data Sheet: Sikadur-25 Lo-Mod EPU."

Sprinkel, M. 1997. "Nineteen Year Performance of Polymer Concrete Bridge." ACI Symposium Publication, 169. https://doi.org/10.14359/5930.

Sprinkel, M. 2003. "Twenty-Five-Year Experience with Polymer Concrete Bridge Deck Overlays." ACI Symposium Publication, 214. https://doi.org/10.14359/12760.

Stevens, R. J., and W. S. Guthrie. 2021. "Scanning Tour of Polyester Polymer Concrete Overlays on Bridge Decks in California." Tran-SET 2020, 287–297. Albuquerque, New Mexico (Conference Held Virtually): American Society of Civil Engineers.

Toufigh, V., M. Hosseinali, and S. M. Shirkhorshidi. 2016. "Experimental study and constitutive modeling of polymer concrete's behavior in compression." Construction and Building Materials, 112: 183–190. https://doi.org/10.1016/j.conbuildmat.2016.02.100.

Transpo Industries, Inc. n.d. "Product Data Sheet: T-17 Rapid Patch."

Vipulanandan, C., and S. Mebarkia. 1996. "Flexural and Facture Properties of Glass Fiber Reinforced Polyester Polymer Concrete." ACI Symposium Publication, 166. https://doi.org/10.14359/1394.

Vipulanandan, C., and E. Paul. 1990. "Performance of Epoxy and Polyester Polymer Concrete." ACI Materials Journal, 87 (3). https://doi.org/10.14359/2187.

Wagner, E. 2021. Kwik Bond Hybrid Composite Synthetic Concrete (HCSC) Material Characterization. 11. Northbrook, IL: Wiss, Janney, Elstner Associates, Inc.

Wagner, E. I., and P. D. Krauss. 2020. Bond Behavior of Reinforcing Steel in Kwik Bond HCSC Material. 15. Northbrook, IL: Wiss, Janney, Elstner Associates, Inc.

Yuan, J., and B. Graybeal. 2014. Bond Behavior of Reinforcing Steel in Ultra-High Performance Concrete. 78. Washington, D.C.: USDOT FHWA.